NASA CR-66069
TRW ER-6819

STRETCH-FORMED ALUMINUM SOLAR CONCENTRATOR

APRIL 1966

Prepared under Contract No. NAS 1-4684 by
TRW Equipment Laboratories
TRW INC.
Cleveland, Ohio
for
NATIONAL AERONAUTICS AND SPACE ADMINISTRATION

NASA CR-66069
TRW ER-6819

STRETCH-FORMED ALUMINUM SOLAR CONCENTRATOR

Prepared under Contract No. NAS 1-4684 by
TRW Equipment Laboratories
TRW INC.
Cleveland, Ohio

for

NATIONAL AERONAUTICS AND SPACE ADMINISTRATION

ABSTRACT

25572

Results of the investigation of the solar concentrator fabrication technique and mounting ring design are presented. Fabrication of a 60 inch diameter concentrator is described which resulted in an optical accuracy of 1.59 minutes and 2.08 minutes radial and circumferential standard deviation of surface errors respectively. Measured specular solar reflectivity is 88% to 90% and the concentrator weight is 10.75 pounds.

CONTENTS

LIST OF FIGURES

LIST OF TABLES

STRETCH-FORMED ALUMINUM SOLAR CONCENTRATOR

TRW Equipment Laboratories
TRW Inc.

SUMMARY

Investigations of the TRW solar concentrator fabrication technique and the optimum mounting ring design have been conducted, and a 60 inch diameter solar concentrator has been fabricated utilizing the resulting improvements in tooling, fabrication process, and configuration.

Stretch forming in the laminar flow filtered air atmosphere provided by newly installed clean air units improves the conditions for application of the lubricant and for a dust free stretching operation.

Previously observed radial joint distortions are due to trimming pressures and the edge distortion condition has been improved by an estimated factor of two through the use of a new trimming tool arrangement and by the design of the radial splice joint. The area lost by this distortion is approximately 6.5%.

Optimization of the surface improvement spray coating has been investigated and a high temperature curing epoxy system is recommended to insure space environmental stability. The newly installed clean air units in conjunction with a two stage curing operation was used to eliminate dust and other particles from the coatings. There were occasional blemishes on the surface in the form of small crators where the coating material did not wet the aluminum. Use of a rotating curing fixture and optimized spraying parameters has eliminated gross orange peel, but a fine orange peel condition remains. Specular solar reflectance measurements for the final hardware are between 88% and 90%.

Optical inspection of the 60 inch diameter mirror shows a geometric quality improvement over previously fabricated stretch-formed mirrors. The measured radial and circumferential standard deviation of surface errors are 1.59 minutes and 2.08 minutes respectively.

The measured weight of the 60 inch diameter solar concentrator is 10.75 pounds resulting in a specific weight of 0.55 lb/sq ft. of intercepted solar flux.

INTRODUCTION

This report covers work accomplished under contract NAS 1-4684 for the research, development, fabrication and delivery of a five-foot diameter stretch formed solar concentrator for NASA, Langley Research Center.

The purpose of the investigations was to develope the TRW fabrication process to a point where one-piece paraboloidal concentrators can be fabricated with geometrical and surface finish properties superior to those obtained in the concentrators previously fabricated by the stretch-formed process.

The basic TRW fabrication technique consists of bonding together stretch formed aluminum segments into a one-piece paraboloidal reflector. This thin gage reflector is stiffened by a structural mounting ring at the outer diameter. To obtain the highly smooth surface finish required for solar reflectors, an epoxy surface improvement coating is applied to the stretch formed segments and subsequently a vacuum aluminized mirror film is deposited to obtain a high reflectivity.

The feasibility of fabricating light-weight solar reflectors by this technique was established in an early contract effort (NAS 7-154). During a second phase contract (NAS 1-3216) the basic tooling and present fabrication facilities were established and a 60 inch mirror was fabricated. In the present work, modifications were made to the existing facilities so that investigations and improvements could be made in the following specific areas:

(1) Stretch forming
(2) Joint distortions due to trimming and bonding
(3) Surface improvement coating technique
(4) Design of a mounting ring member

RESEARCH & DEVELOPMENT INVESTIGATIONS

The research and development portion of the contract work consisted of investigations in the basic fabrication process which would improve the geometric and surface finish properties of the one-piece paraboloidal concentrators. Also, the mounting ring which is used to reinforce the mirror was investigated by designing, fabricating and testing several promising ring configurations.

Fabrication Process Investigations

Stretch forming - The stretch forming setup is shown in figure 1 and consists of the glass master paraboloidal form on a support base, hydraulic actuating cylinders, and the clamping jaws. The glass paraboloid is a surplus search light mirror which serves as an inexpensive master form with relatively high geometric accuracy. As shown in figure 1a, the flat aluminum stock is clamped in the jaws and stretched over the master form. When loaded to the plastic region, the aluminum permanently stretches and accurately replicates the paraboloidal shape.

In conjunction with this forming process, the objective of the present work was to devise a suitable technique for keeping the forming tool and the aluminum stock free of dust during stretching and to establish the optimum method for application of the dry lubricant which is used in the forming process. To this end, the portable filtered air units shown in figure 1b were used in the stretch forming area to control the air flow and dust condition during application of the lubricant and during the stretching operation.

During the investigation, modifications were made to the stretching tool apron to improve the stretch approach angle. Also, a guide bar and drill bushings were added to the apron area to allow the drilling of reference piloting holes in the stretched sheets for accurate location of the parabolic shape in subsequent operations.

The material used in the fabrication of TRW's stretch formed solar concentrators is 3003-0 Specialty Bright aluminum alloy which requires special mill rolling to obtain a superfine finish not exceeding 2 micro inches rms. Since this special material has a four month delivery, other sheet material which is available in stock was purchased for the early evaluation portions of the contract. This material consisted of .016 inch thick stock with a mill finish (20 micro inches rms) which was used for the joint distortion evaluations and the mounting ring markoff tests. "Bright one side" stock .020 inch thick was obtained to be used in the initial evaluations of the surface improvement coating task. This is the closest gage material in "bright one side" which is available from stock. When the specially rolled stock was obtained, additional stretch forming was performed to provide panels for the optimization of the surface coating technique.

The twelve stretch operations which are summarized in Table I were performed in conjunction with the clean air units and they constituted the major portion of the investigation effort. This material was then used in the final

TABLE I

STRETCH FORMING INVESTIGATION SUMMARY

Gage (inches)	Lube System	Method	Results
.016 (mill)	Fluorocarbon dry film A	Pour on tool	Streaks
.016 (mill)	1 Teflon dry film 1 Ethyl Alcohol	Wipe on tool	Too much lube - piles up & dimples stock
.020 (bright)	Fluorocarbon dry film B	Spray tool with gun Buff off	Not a full stretch - piles up
.020 (bright)	Teflon dry film	Wipe on stock	Too much lube - piles up
.020 (bright)	1 Teflon dry film 3 Ethyl Alcohol	Wipe on stock Buff off	Piled up only at scratches
.016 (Special)	1 Teflon dry film 3 Ethyl Alcohol	Wipe on stock Buff off	Stock galls on tool
.016 (Special)	1 Teflon dry film 3 Ethyl Alcohol	Wipe on stock & tool Buff off	Lube piles up
.016 (Special	1 Teflon dry film 3 Ethyl Alcohol	Wipe on tool Buff off	Stock galls on tool
.016 (Special)	1 Teflon dry film 3 Ethyl Alcohol	Apply 2 coats to stock & tool. Hard buff	Stock galls on tool
.016 (Special)	Silicone wax	Apply to stock & tool Buff lightly	Wax piles up & dimples stock
.016 (Special)	Silicone wax on tool Teflon on stock	Hard buff tool Buff stock	Stock dimples & scratches
.016 (Special)	Fluorocarbon dry film B	Spray tool with gun Medium buff	No scratches - min. dimples

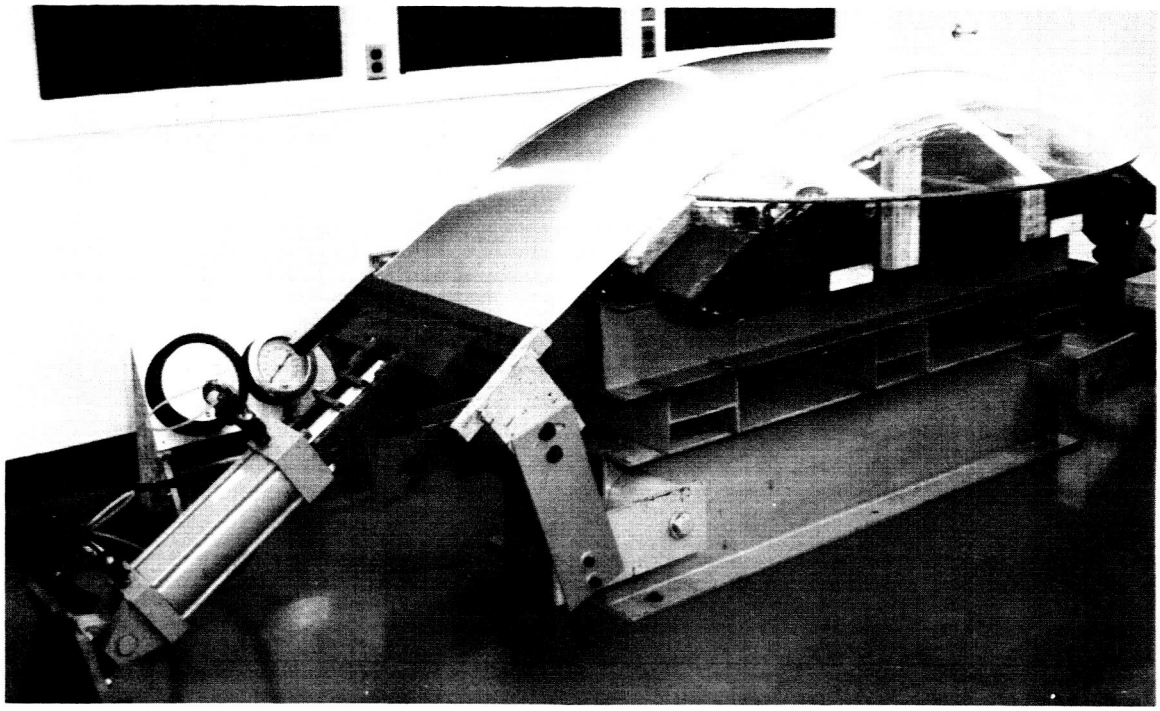

FIGURE 1a

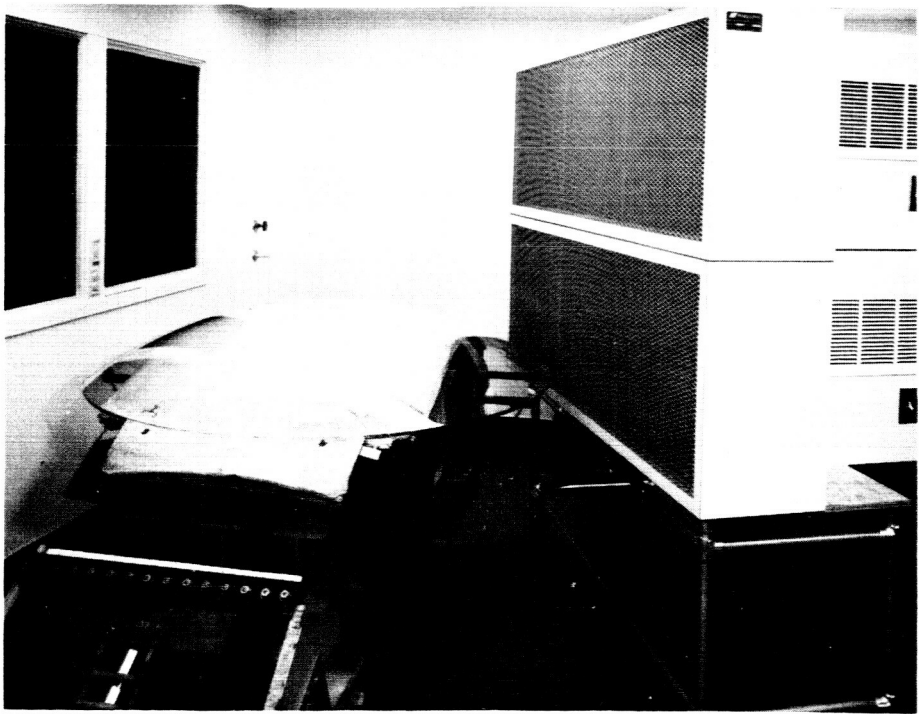

FIGURE 1b
STRETCH FORMING ARRANGEMENT

surface coating and trim evaluation tasks. The major conclusions drawn from these results of the stretch investigation are as follows:

(a) The filtered air units are a definite aid in keeping the tool and stock free of dust, but final inspection with a bright light and a final air blow off are required.

(b) Too much lubricant will pile-up under stretching pressures and dimple the stock; while too little will cause the stock to gall on the tool.

(c) The optimum thickness and uniformity of the lubricant can best be obtained by spray coating the tool and using a final buffing operation.

(d) Final cleaning and inspecting of the stock before placing on the tool should be performed in front of the filtered air units.

(e) Imperfections in the flat stock will magnify by piling-up lubricant which then marks-off under the stretching pressure.

The use of a spray gun rather than the aerosol spray cans as previously used provides a more uniform coating since only several wide pattern passes are necessary; also, particle build-up on the spray nozzle is minimized.

The finalized process which was used to stretch the final hardware for the 60 inch mirror consists of spray gun application of the fluorocarbon dry film lube to the tool with a final medium buffing operation to obtain the proper uniformity and thickness of lubricant. The detailed process which was used is presented in Appendix A.

The geometric accuracy obtained by this method of replication will be discussed in a later section.

Surface improvement coating. -Ideally the reflector surface should have the smoothness of an optical flat. Special mill runs are capable of finishing aluminum sheet to less than 2 micro inch rms. However, during the stretch forming process grain distortions increase this value to about 4-6 micro inch rms and the surface has a dull appearance. Epoxy coating the formed sheets results in an improved substrate for the subsequent vacuum aluminizing.

In the coating process a thin epoxy layer is applied by spraying the stretch formed panels. The coating material must satisfy two primary functions. It must be stable in the space environment and it must provide a specular or glass-like surface.

Two epoxy coating materials were considered during the present contract work - a low temperature and a high temperature curing epoxy system. The low temperature epoxy displayed excellent leveling characteristics, but it was found to soften and distort at the elevated temperatures which can be anticipated for typical solar concentrator environments. The higher curing temperature epoxy is recommended for a stable solar mirror substrate; and therefore, the present coating investigation was centered on the high temperature epoxy system.

In conjunction with the epoxy spray coating of the stretch formed aluminum panels, the following sources of blemish have been investigated to obtain a process which results in a highly specular surface:

Air borne dust and lint
Solid inclusions in the epoxy
Pin holes or non-wetting areas
Orange peel
Runs and streaks

One of the major sources of surface blemishes which was observed in previous work was dust in the form of lint and grains. High air volume requirements during spray operations raised the dust level approximately two orders of magnitude. Prior investigations revealed that a coating could effectively mask particles of sizes up to one-half its thickness. Lint on the other hand produced irregular shaped distortions and could not be covered.

To eliminate the dust problem, the existing spray and exhaust equipment, which has been described in reference 1, was modified to include two laminar flow clean air units installed at the inlet of the spray booth - see figure 2. The total frontal area is six feet wide and four feet high almost equaling the spray booth opening. An adapter was built to provide an enclosure of the automatic spray equipment and a transition and seal from booth to the clean air units. The laminar flow air units supply sufficient air, at an average velocity of 200 feet per minute, to provide a slight positive pressure inside the spray booth during the spraying operation. The clean air units are mounted on a portable frame so that they can be moved for access to the spray booth. Also, the portable arrangement allows easy utilization of the clean air units in the stretch forming area as was previously discussed.

By employing the laminar flow clean air units and using extreme care in cleaning and handling of the parts, the coated panels show only occasional occurrence of dust and lint particles.

Solid, lump-like particles which were not air borne were also observed in the coating. These lumps were investigated under a microscope since naked eye examination revealed only the protrusions on the surface. Some contained fragments of what appeared to be cured coating material. These particles with flat and ragged sides could easily be identified because of a slight difference in color and index of refraction. Others appeared as a pinhead with a long curly tail extending about .008 inch. Moisture content of the coating components and the possibility of condensation from the air were investigated as possible causes of these inclusions

The possible effect of the relative humidity was also investigated. Solvent evaporation could lower the temperature sufficiently to condense water onto the surface. A thermocouple imbedded in freshly applied coating material showed only a slight change in temperature. Since the relative humidity is held to a maximum of 50% in the work area, a drop from 72° F to 60° F would be required to reach dew point conditions. Although moving air in the spray booth would tend to lower the temperature more than in still air the effect is insignificant. This is plausible because the solvent evaporation takes place over a prolonged period. It was concluded that under the prevailing conditions,

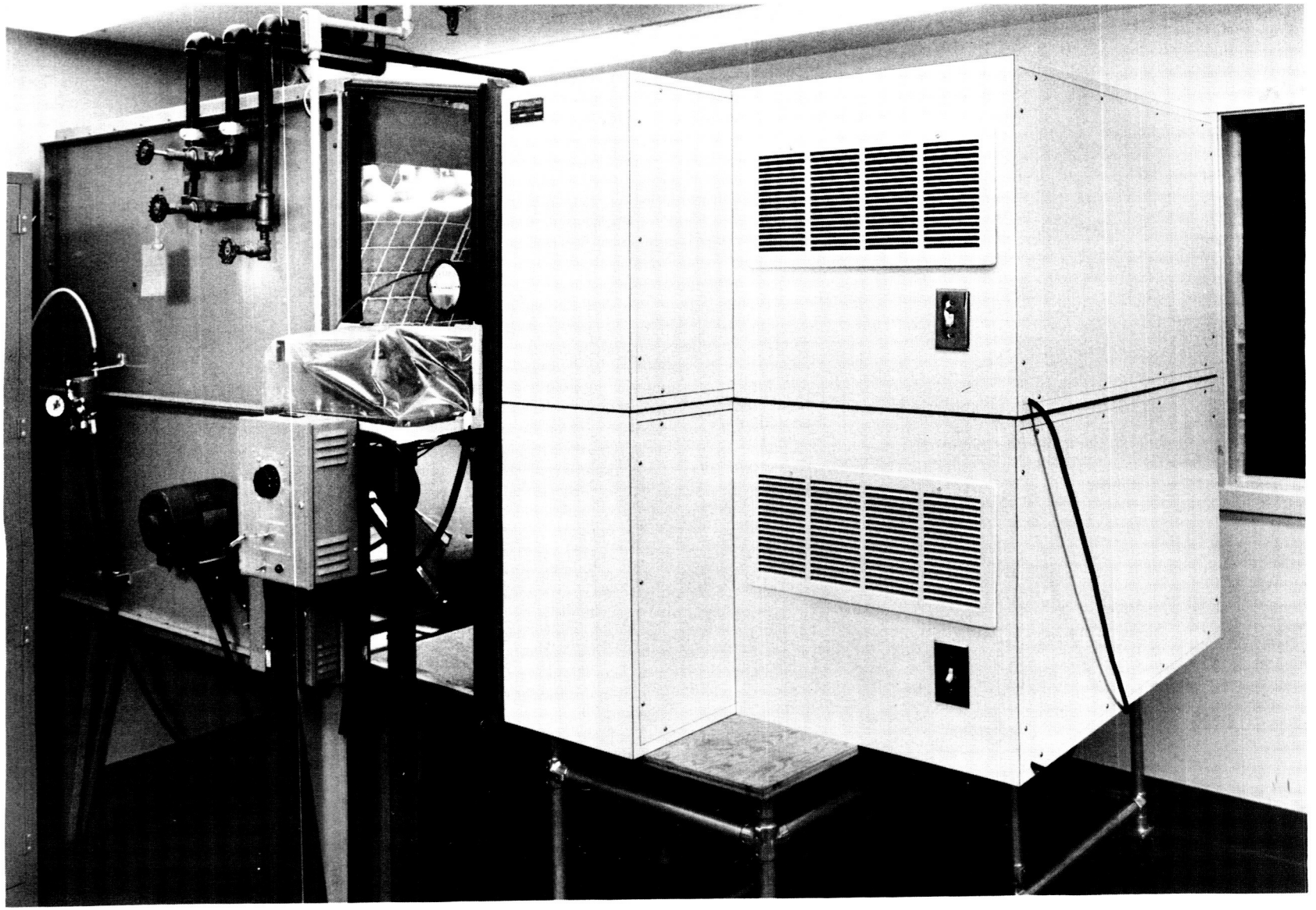

FIGURE 2
AUTOMATIC SPRAYING FACILITY

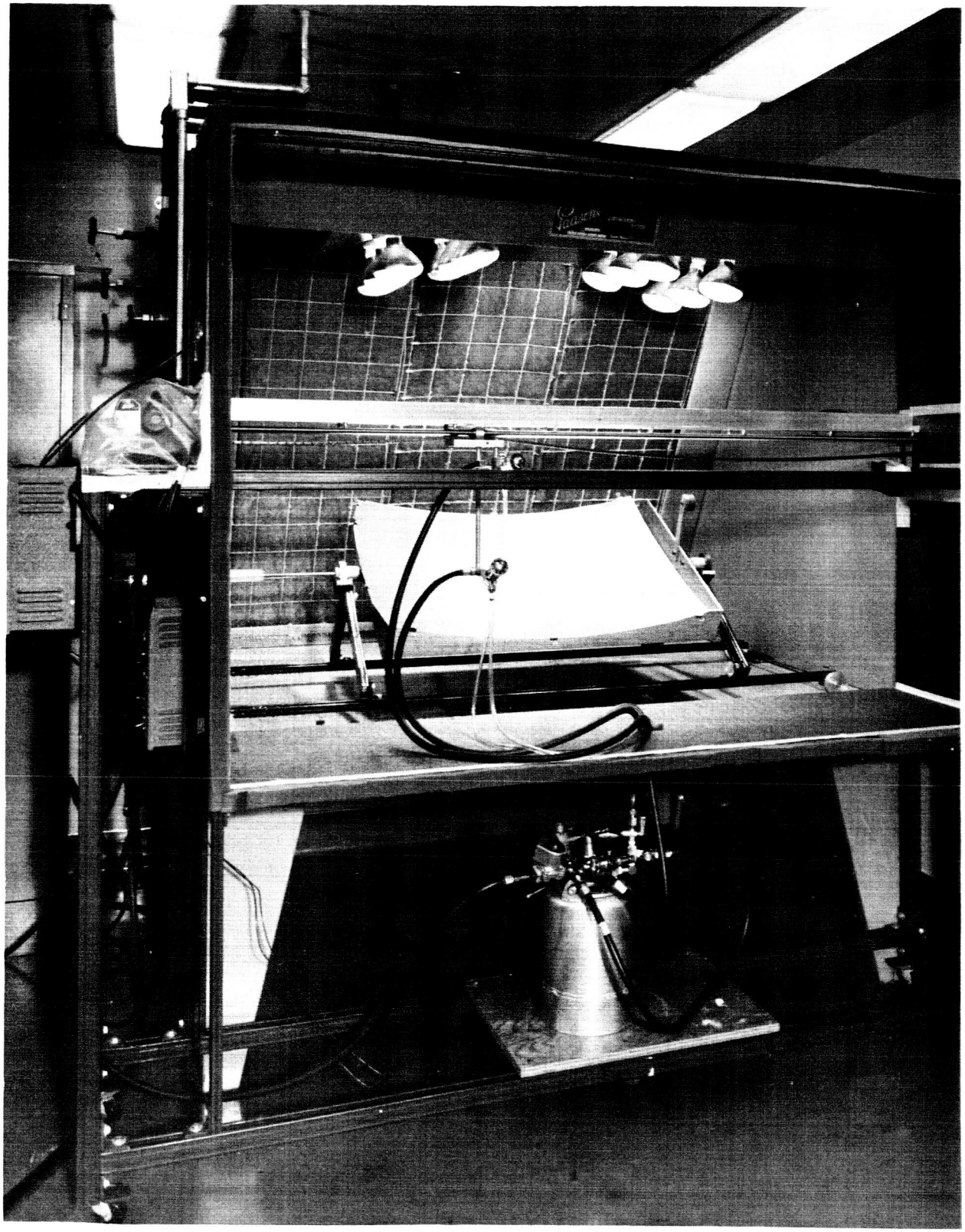

FIGURE 3
AUTOMATIC SPRAYING & PRE-CURING SETUP

water has no detrimental effect.

Further investigations into the cause of the lump-like blemishes indicated that the agents must be in the coating material itself. Fittings and guns of the spray equipment were cleaned and new, clear plastic hoses installed. Also, the coating material was thoroughly mixed, allowed to soak and filtered. Almost all inclusions were absent on the next piece but recurred in increasing numbers at subsequent sprayings despite a solvent flushing of the system after each use. Examining the insides of hose and fittings showed that the epoxy left a thin residual film and some heavy fillings at joints which were at various stages of curing. During subsequent spraying some of these residues broke loose and were deposited with the coating. From these investigations it was concluded that the previous method of cleaning by flushing is not adequate; therefore, the process was modified such that after each spray all fittings are removed, cleaned, and new fluid hoses are installed.

Spray coating optimization. -The control of runs, orange peel, and pinholes as surface blemishes in the coating process are all related to the many spray system parameters.

In the coating process, epoxy coating material is thinned with a mixture of solvents for spray application to the formed panels. The solvents reduce the viscosity so that the coating can be sprayed bubble free. High vapor pressure solvents quickly increase the coating viscosity after spraying due to the fast evaporation rate and thereby reduce the tendency to sag or run. Slow evaporation of the others allows enough time for leveling to eliminate orange peel. The proper leveling is also associated with the rotating curing arrangement and the curing cycle. Previously, the parts were sprayed and placed in a tray to cure. This was not the best method since the natural tendency of the material was to flow to the lowest point producing a puddle and streaks. A rotating fixture was designed and built so that the part could be sprayed and immediately rotated Since rotation would change the surface attitude continuously flow tendencies would be arrested. Also, heat lamps were installed in the spray booth for pre-curing of the coating while in the filtered air environment. Figure 3 shows the rotating fixture and pre-curing lamps arrangement.

In conjunction with this spraying and curing facility the basic spray coating technique was investigated. This investigation consisted of a systematic program of small specimen and full panel spray coating to optimize the major spraying parameters.

One of the major parameters is the solvent additives required to obtain proper spraying and leveling characteristics. Also investigated as an additive was a urea-formaldehyde resin which is recommended by the manufacturer as a leveling or flowing agent when added to the epoxy coating material. The following nine additives were investigated for their basic compatibility with the epoxy coating material.

Additive	Classification	Relative Evap. Rate (Butyl Ace. = 100)	Evaporation Classification
Acetone	Solvent	1160	Fast
Benzene	Diluent	630	Fast
MEK	Solvent	572	Fast
Toluene	Diluent	240	Medium
MIBK	Solvent	165	Medium
Xylene	Diluent	70	Medium
Butanol	Coupler	45	Slow
2-Butoxyethyl	Solvent	3	Slow
Resin	Flowing agent	-	-

It is seen that this selection provides 4 solvents, 3 diluents and 1coupler; while they also have a range of volatility which gives 3 fast, 3 medium, and 2 slow. The compatibility of these additives was investigated by mixing with the epoxy - both individually and in certain combinations. The mixtures were quite soluble immediately upon mixing but some displayed gelling characteristics after a period of time. The term "gel" is used here to describe a condition of observable fluid motion such that when stirred, streaks or clouds were seen in the transparent mixture. In no case did the mixture become a firm gel or noncompatible gel; and none of the mixtures showed tendencies for separation even after several days.

Based upon these compatibility tests, the following four additives were selected for major consideration in the small specimen spray tests.

MEK	- fast
Toluene	- medium
MIBK	- medium
2-Butoxyethyl Acetate	- slow

These solvents were selected based upon the absence of any fog condition and the tendency not to gel.

The next step in the coating optimization was to investigate the effect of these solvents upon the spray characteristics of the epoxy coating by spraying 8 x 10 inch specimens. These specimens were cut from stretch formed panels and cleaned for spraying.

Fifty small specimens were spray coated in the spraying facilities previously described. These specimens and their resulting characteristics are presented in Appendix B. The first 32 specimens used various combinations of MEK, toluene, MIBK, and 2-butoxyethyl acetate to investigate leveling characteristics, epoxy to solvent ratios, and rotational curing speed. The remaining 18 specimens were used to investigate the curing cycle characteristics. Also, the resin leveling agent and several other solvents were investigated.

All specimens were aluminized and visually inspected to determine their comparative leveling characteristics. Thermal testing was performed on the 12 best aluminized small specimens. The temperature of these specimens was increased in increments of 50°F to 300°F maximum. Cracking of the coating was observed on only one specimen. The remainder of the specimens

showed no indications of crazing or cracking - indicating the thermal stability of the high temperature epoxy system in combination with the vacuum deposited mirror coatings. A specimen with the same coating which cracked but with a longer cure cycle was thermally tested to 300°F and it displayed no cracking. For this reason, the cure time was increased for the final spray tests.

To finalize the coating process, four full size panels were sprayed and aluminized using the most promising two processes which were established in the small specimen spray tests. These full panels consist of one-half of a stretch formed sheet. The resulting finalized process which was then used in fabricating the 60 inch mirror is detailed in Appendix A and the important parameters are as follows:

Spray mixture - 1.7 parts epoxy
1.0 parts 50% MIBK, 50% 2-butoxyethyl

Spray settings - Air pressure - 75 psi
Tank pressure - 10 psi
Flow setting - 100
Pattern setting - fan shape
Gun travel - 50 fpm

Drying rotation - slow (12 rpm)

Cure - Precure drying with heat lamps - 12 hrs.
Oven cure - 150°F 3 hrs.
300°F 2 hrs.

This combination of spraying parameters allows the compound curvature full panels to be coated without runs, and the gross orange peel tendency has been eliminated by the use of a very low volatility solvent (2-butoxyethyl acetate) which allows the coating time to level before evaporating. However, a very fine orange peel condition which was observed on the small specimens was also present on the full panel sprays. It is anticipated that this fine orange peel will affect primarily the specular reflectivity of the mirror surface. The specular reflectivity which was obtained by this process was measured on the final hardware panels and will be discussed in a later section.

As discussed previously, the surface condition which was observed on the full panels shows only occasional occurrence of dust and entrapped particles. Also observed, however, is a surface discontinuity termed "pin holes" or crators which are apparently due to random nonwetting spots on the panel. Efforts to eliminate them on the full panels included changing the panel cleaning procedure, changing the epoxy viscosity, and variation of several spraying parameters. It has been concluded from tests with other substrates and from microscopic examination of the pin holes that the epoxy-solvent combination which gives the least orange peel condition is a poor wetter, and that the origin or nucleus of these spots may be the very small dust and foreign particles which previously have been covered by the epoxy-solvent systems.

Sector joint distortion. -In previously fabricated stretch formed solar reflectors, a surface distortion along the radial joints of the assembled sectors has been observed and reported (ref. 1). The possible sources of this edge

distortion are:

(a) A trimming pressure which distorts the edge when the sector is cut from the stretched panel.

(b) Stress release which causes distortion when the trimming operation relieves a possible residual stress across the part thickness.

(c) Adhesive bonding characteristics of the radial joint splice.

Since the edge distortion has been observed to be present prior to the joint bonding, it is obvious that source (a) or (b) must be present and that the bonding (c) can then further affect the joint condition.

The sectors are cut from the stretch formed panels by a high speed slitting saw as shown in figure 4. The purpose of this portion of the contract work was to investigate the nature of the joint distortion. The following procedure was used:

(a) A new trimming tool was replicated from the master parabolic tool. This tool includes piloting reference pins for accurately repositioning the stretch formed panel. The new tool provides better support for the panel during the cutting operation. The trimming tool and a panel which has been radially cut is shown in figure 5 with the outer diameter cutting arrangement.

(b) An "as stretched" panel was trimmed on the new tool for comparison with a sector which was trimmed from a "stress-relieved" panel.

(c) Several cuts on stretch formed material were made by electrical discharge machining EDM, commercially called ELOX, see figure 6. These cuts were then compared to the slitting saw method as a check on trimming pressure versus stress relief. If the edge distortion is due to the stress relief possibility, then similar distortion should be observed regardless of the method of trimming.

(d) Sample radial joint splices were made of both the "as stretched" and the "stress-relieved" sectors for comparison of the before and after condition.

During the early investigation period, a total of six sectors were trimmed to size for the various comparisons. Observation of the edge distortion characteristics were made by viewing the reflection of a diffuse source of light from approximately the focal point region. At this point any edge distortions are apparent as contrasting shadows. Typical inspection photographs for recording the edge distortion characteristics are shown in figure 7. This shows the "as stretched" trimmed sector before and after the sample radial bond splice was made.

Based upon observations and comparisons as outlined above, the major conclusion is that joint distortions are primarily due to trimming pressures associated with the slitting saw method of cutting. One of the observed results which confirms these conclusions is that there is no major difference

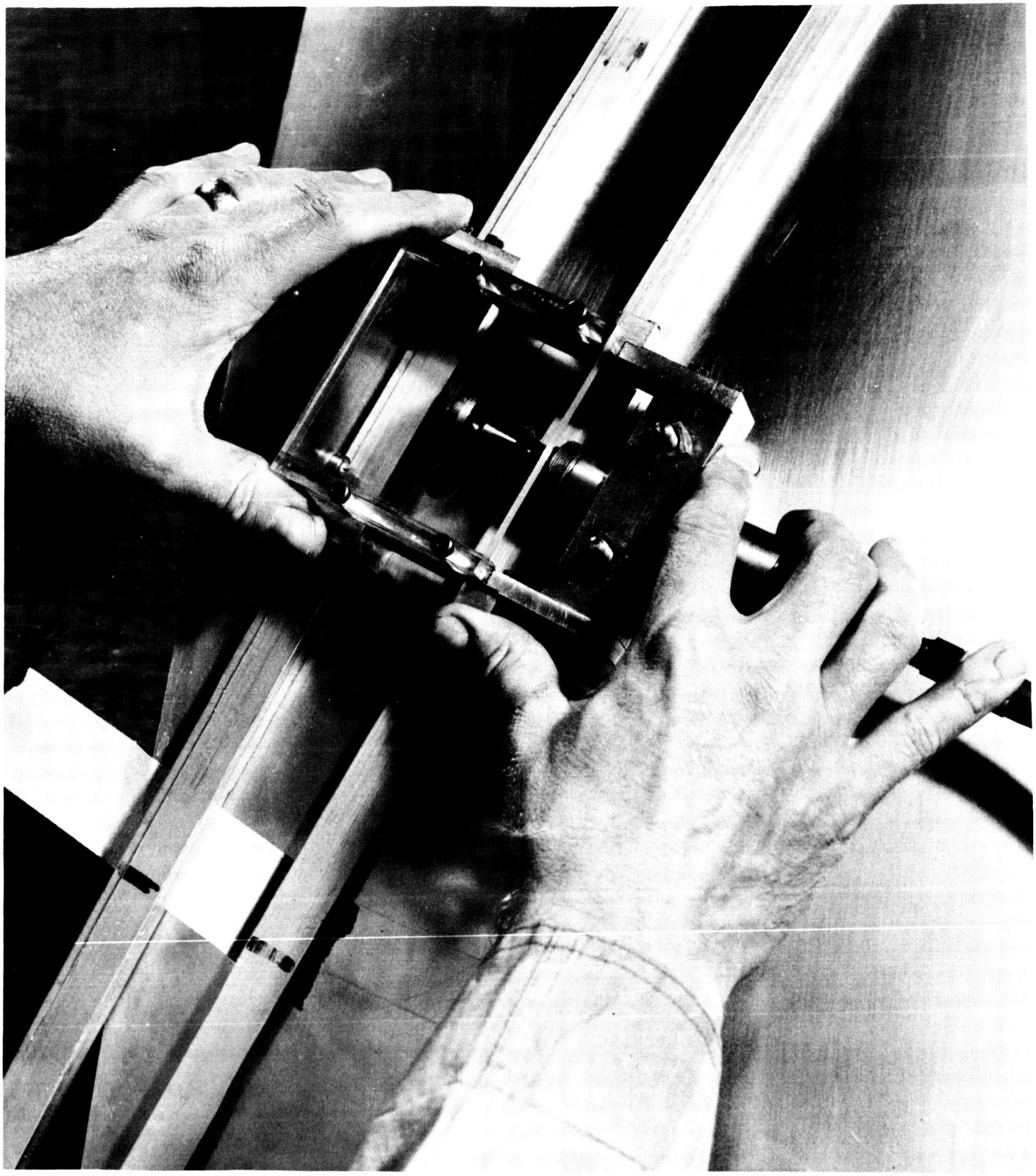

FIGURE 4
TRIMMING SAW ARRANGEMENT

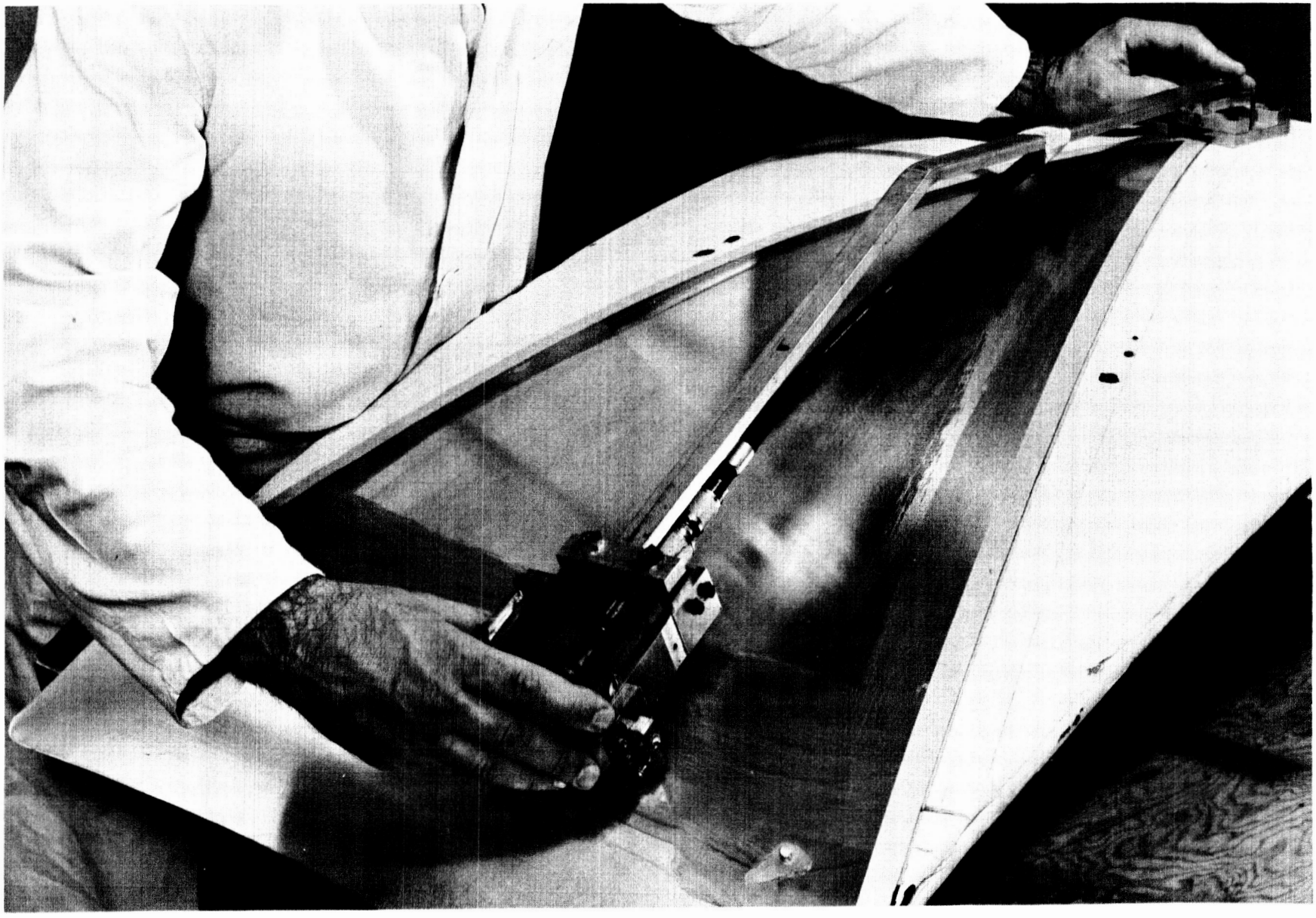

FIGURE 5
TRIMMING TOOL ARRANGEMENT

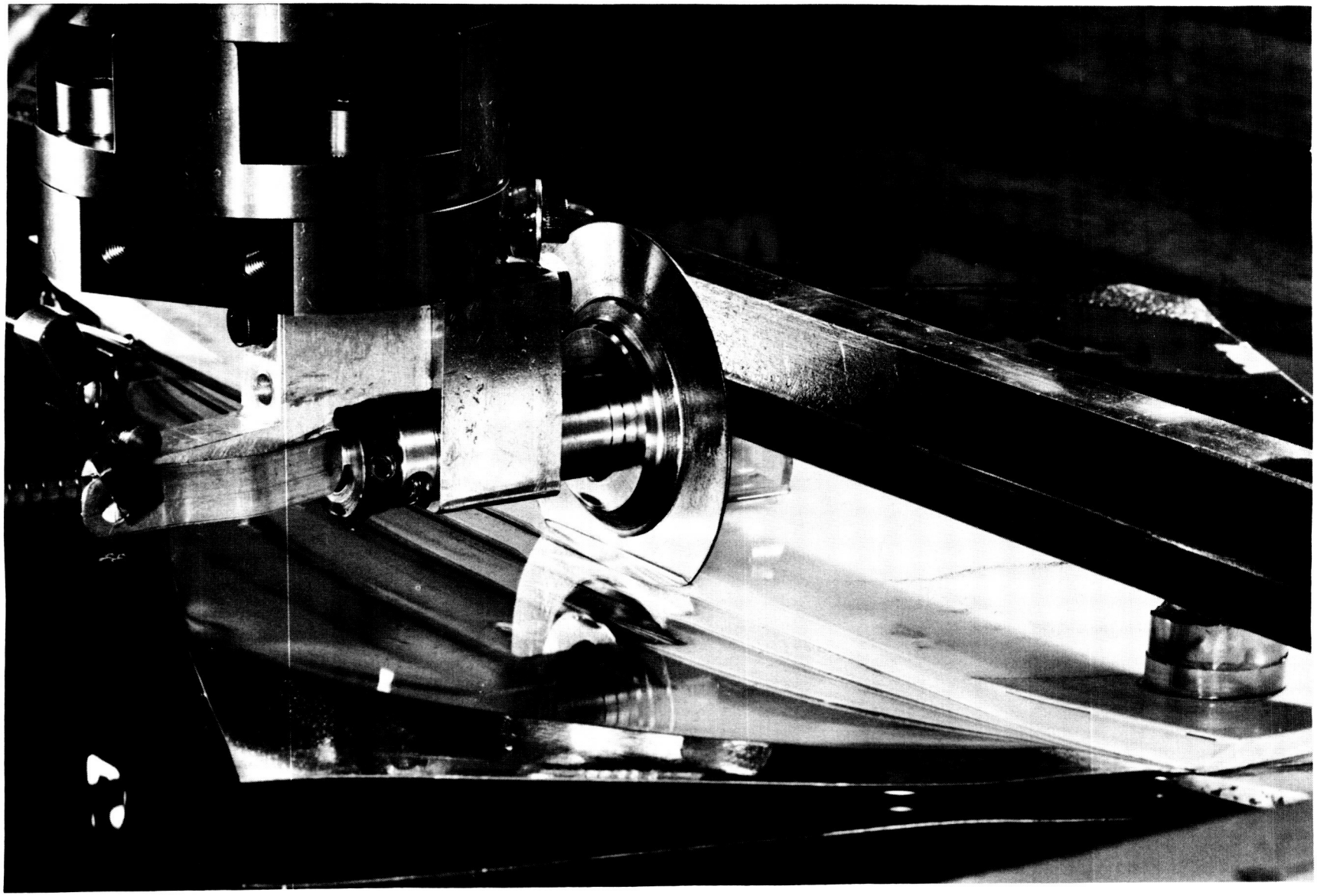

FIGURE 6
EDM TRIMMING SETUP

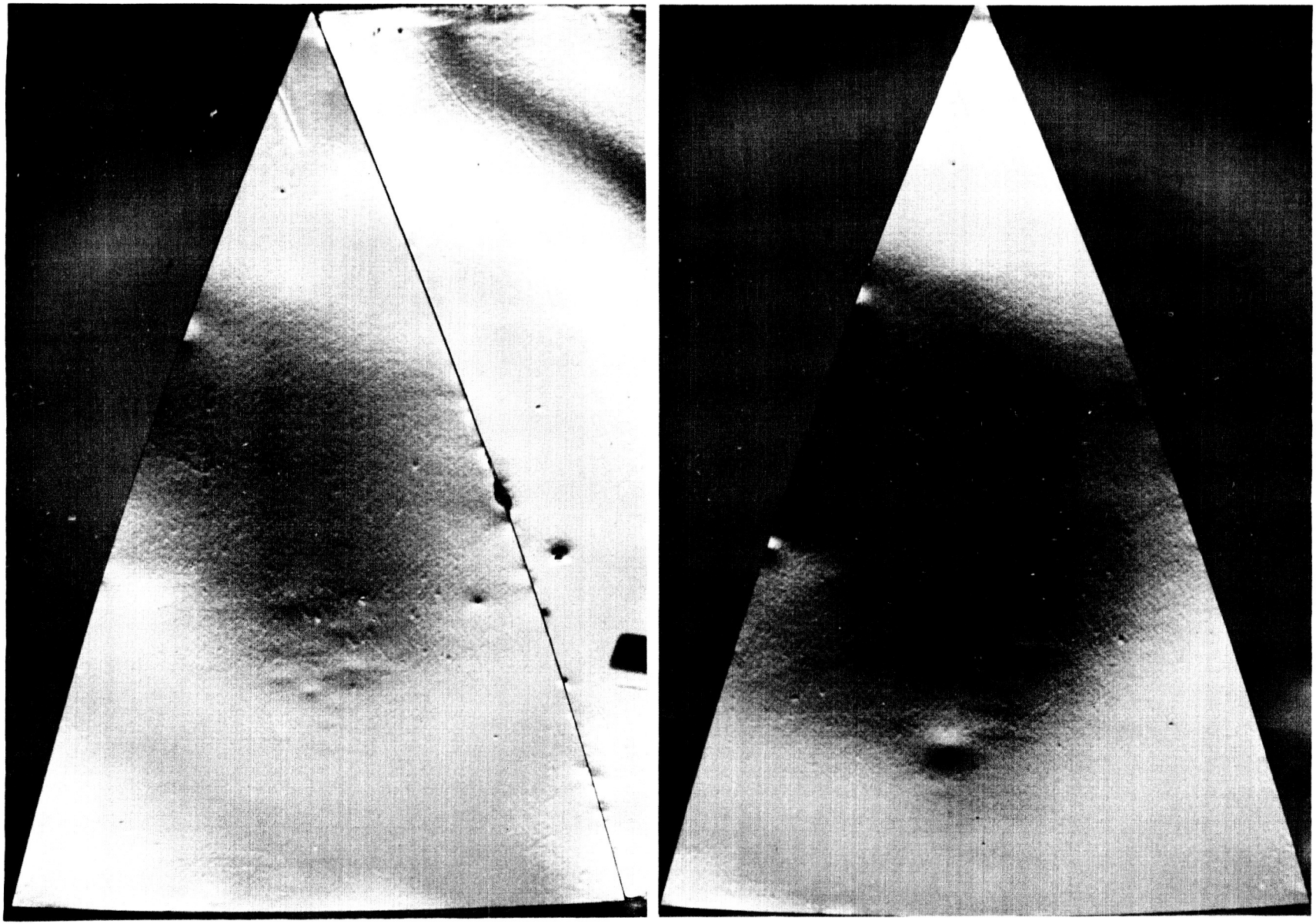

FIGURE 7
EDGE DISTORTION SPECIMENS

between the "as stretched" and the "stress-relieved" edge distortions.

The EDM cut parts also confirm the lack of a residual stress condition in the part since the edge distortion for these cuts was observed to be very low. The EDM cuts, however, cause chipping of the epoxy coating and aluminized surface along the edge. Also, the oil bath associated with the EDM process results in a film of oil which is difficult to remove from the mirror surface.

When the .016 inch thick specially rolled aluminum stock was received, the new trimming tool arrangement was used to final cut the stretch formed panels. The resulting range of observed edge distortion is shown in figure 8. Also plotted in this figure are several curves which represent the theoretical edge distortion characteristics if the distortions were caused by an internal residual stress. This edge effect characteristic is given by Timoshenko (ref. 2) as,

$$\frac{dw}{dx} = \frac{M}{\beta D}\left(e^{-\beta x}\right) \cos \beta x$$

where w = radial displacement

x = axial coordinate measured from the edge

D = flexural rigidity $= \dfrac{E t^3}{12 (1-\mu^2)}$

$\beta^4 = \dfrac{E t}{4 R^2 D}$

t = Thickness of the shell

R = radius of curvature

μ = Poisson's ratio

$\dfrac{dw}{dx}$ = slope of the edge distortion

If there were an internal residual stress distribution in the stretch formed sheets, this would mean that the outer fibers are stressed differently resulting in an effective edge moment (M) released when the panel is cut. It is seen that the observed edge distortion characteristic is different from what would be expected for a residual stress condition - confirming the conclusion that the edge distortion is mechanically introduced by the saw trimming operation.

Since the edge distortions shown in figure 8 are for the free trimmed edge, the distortion can be restrained by the adhesive bonded radial splice joint in the final concentrator assembly. A brief investigation was conducted to optimize this radial joint design. This consisted of bonding trimmed sectors together with various splice strip designs. The configurations tested and the resulting restraint which was achieved is shown in figures 9 and 10. The double strip design shown in figure 10 was used in the final design of the 60 inch concentrator. The radial edge distortion characteristics which were observed in the final hardware will be discussed in a later section.

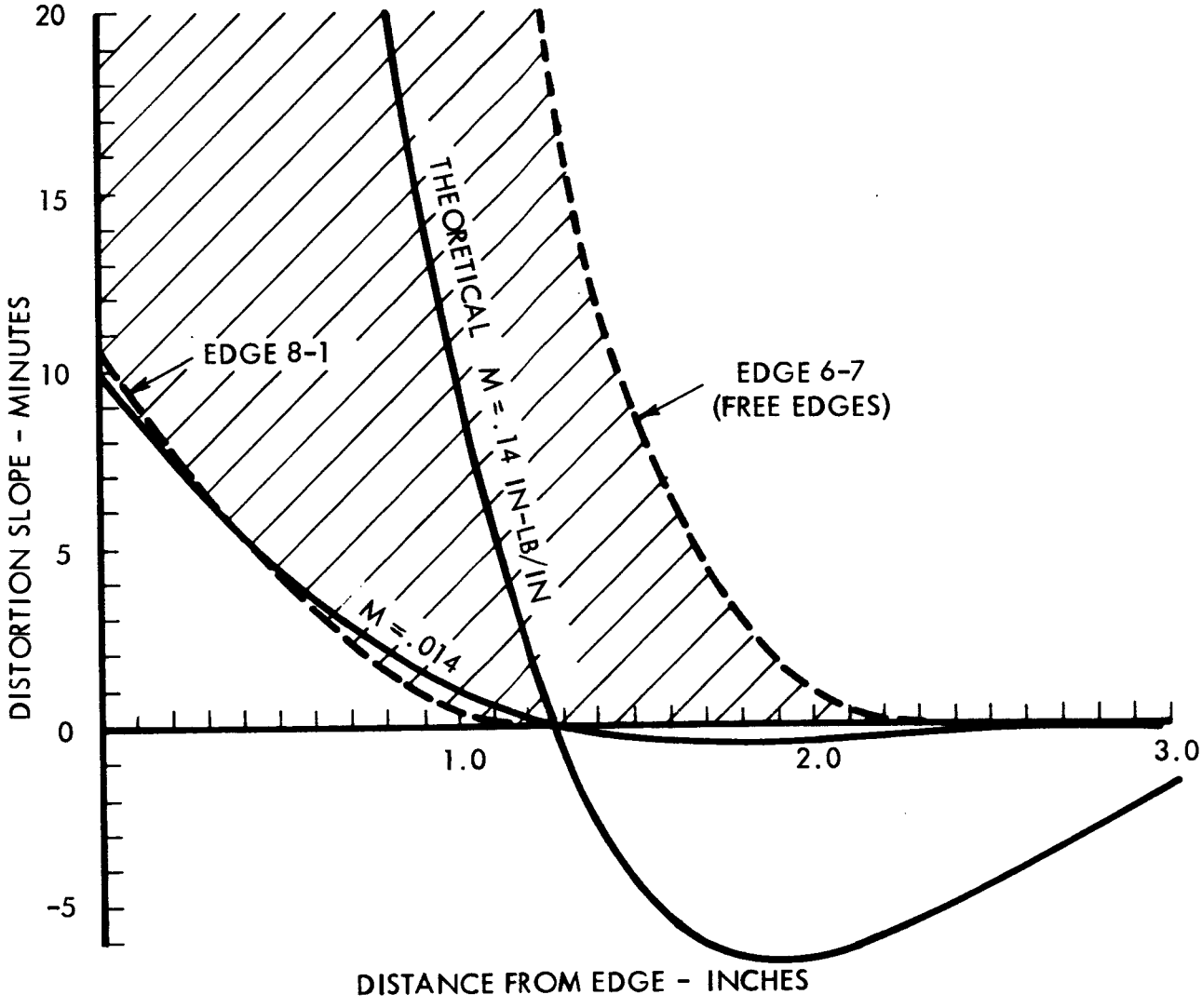

FIGURE 8
RANGE OF EDGE DISTORTIONS

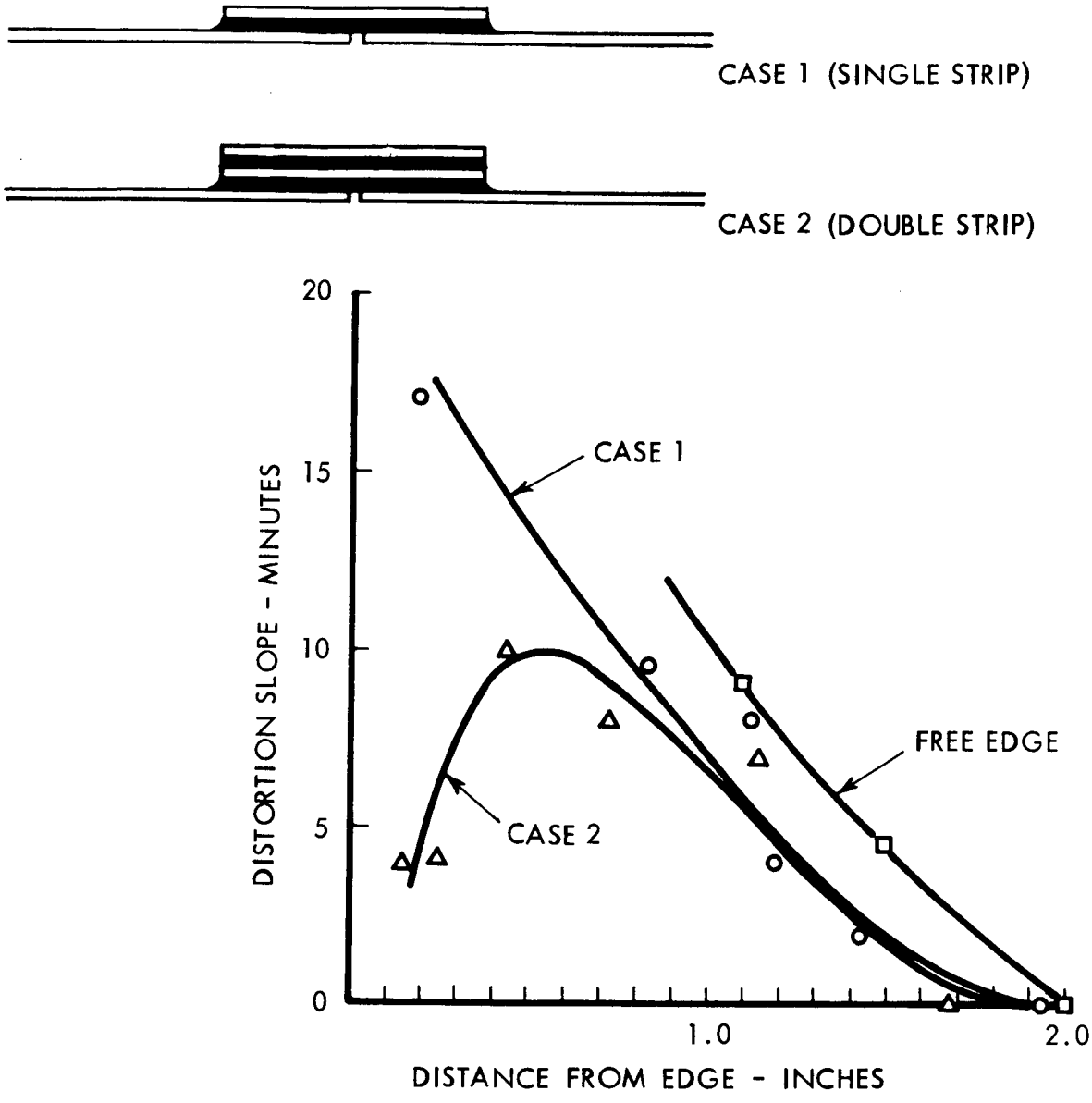

FIGURE 9
EDGE DISTORTION CHARACTERISTICS

CASE 1 (SINGLE STRIP)

CASE 2 (DOUBLE STRIP)

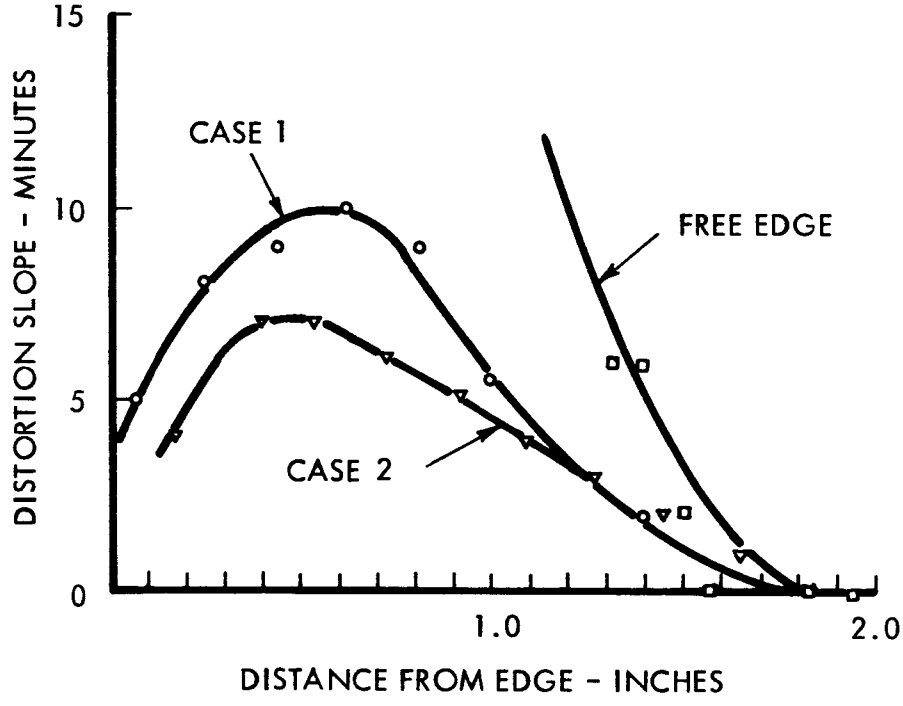

FIGURE 10
EDGE DISTORTION CHARACTERISTICS

Mounting Ring Investigation

The purpose of this task is to design a mounting ring or torus for the solar concentrator. To aid in this design, sample rings were fabricated and evaluated for surface quality of the shell face at the ring-shell junction and for static load capacity of the mounting fixture-ring configuration. The major specifications for the design are that the ring or torus and fixtures in combination with the shell must be capable of withstanding 10 G axial acceleration and 2 G transverse acceleration. The torus shall not be larger in diameter than the diameter of the reflective surface of the concentrator. Also, the torus shall have three equally-spaced mounting fixtures.

Sample Ring Designs and Analysis

The load criterion. -For design purposes, the loading is considered to be the 10 G axisymmetrical acceleration experienced by both the concentrator and the support ring. Meridional forces of magnitude (see ref. 3)

$$N_\phi = \frac{2}{3} fp \frac{1 - \cos^3 \phi}{\sin^2 \phi \cos^2 \phi}$$

will exist in the shell where

f = focal length

p = pressure or weight per unit of shell surface

ϕ = angle between axis of symmetry and normal to the surface

For $p = .020$ psi which is equivalent to a 6-pound concentrator shell undergoing 10 G acceleration, the meridian force at the rim reduces to $N_\phi = 0.65$ pounds per inch. This load is imposed on the ring, in addition to the inertia load of the ring itself. For the ring, assume a mean diameter of 58 inches and a weight of 6 pounds. This is equivalent to a loading of 0.33 pounds per inch of ring circumference. The shell edge force required for equilibrium, the reaction on the support ring and the ring load are shown in figure 11.

The two ring concepts. -Two ring configurations were designed and detailed for the partial ring tests. One design is a torus of circular cross section with a cylindrical skirt placed between the torus and the concentrator shell. The second design is a honeycomb stiffened built-up section of triangular cross section. The cross sections are shown as figures 12a and 12b. The configurations are limiting designs in that the attachment area to the shell is a minimum in the tube-torus-skirt design whereas in the triangular ring design the attachment area is considerably larger but assumes that ring to shell mark-off can be eliminated.

Tube-torus-skirt analysis. -The stresses are due to forces indicated in figure 11 imposed on the ring cross section shown in figure 12a. The indicated relationships between loads and forces or moments can be found in Roark

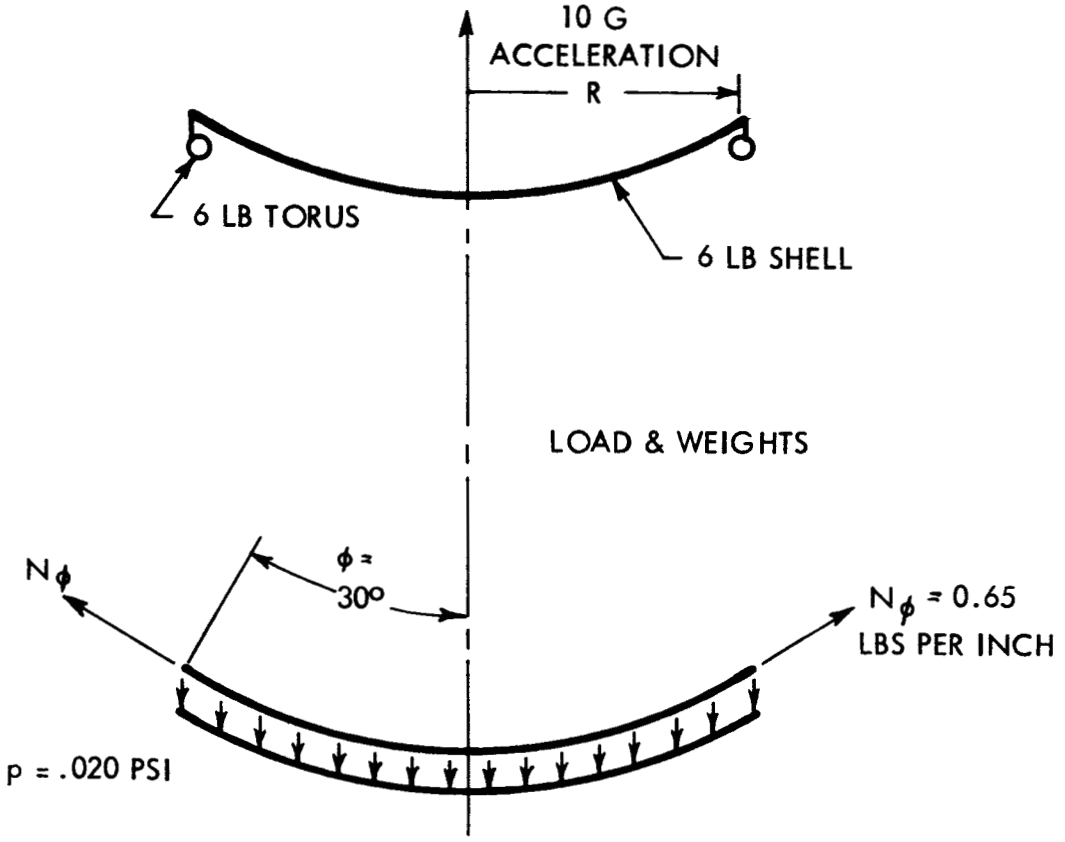

SHELL EQUILIBRIUM

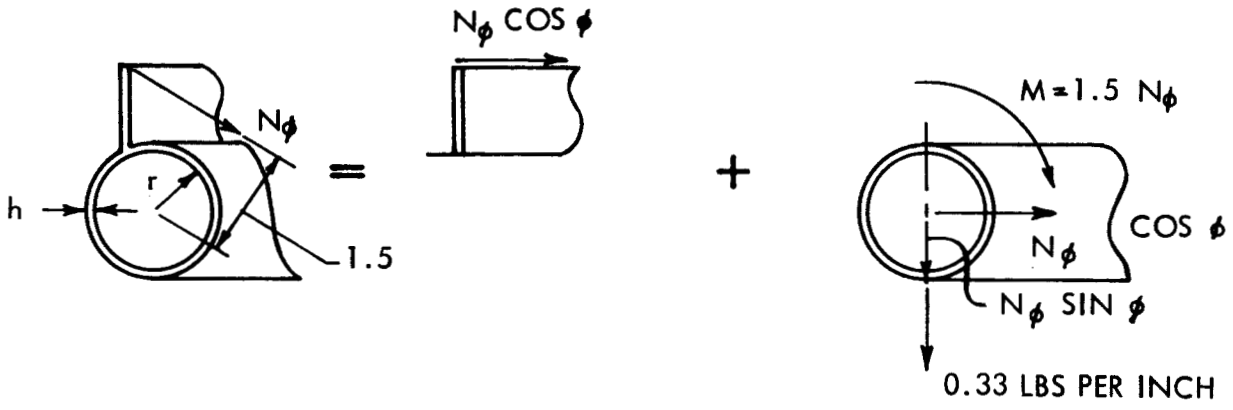

FORCES ON SKIRT AND TORUS

FIGURE 11
LOAD AND FORCE DIAGRAM

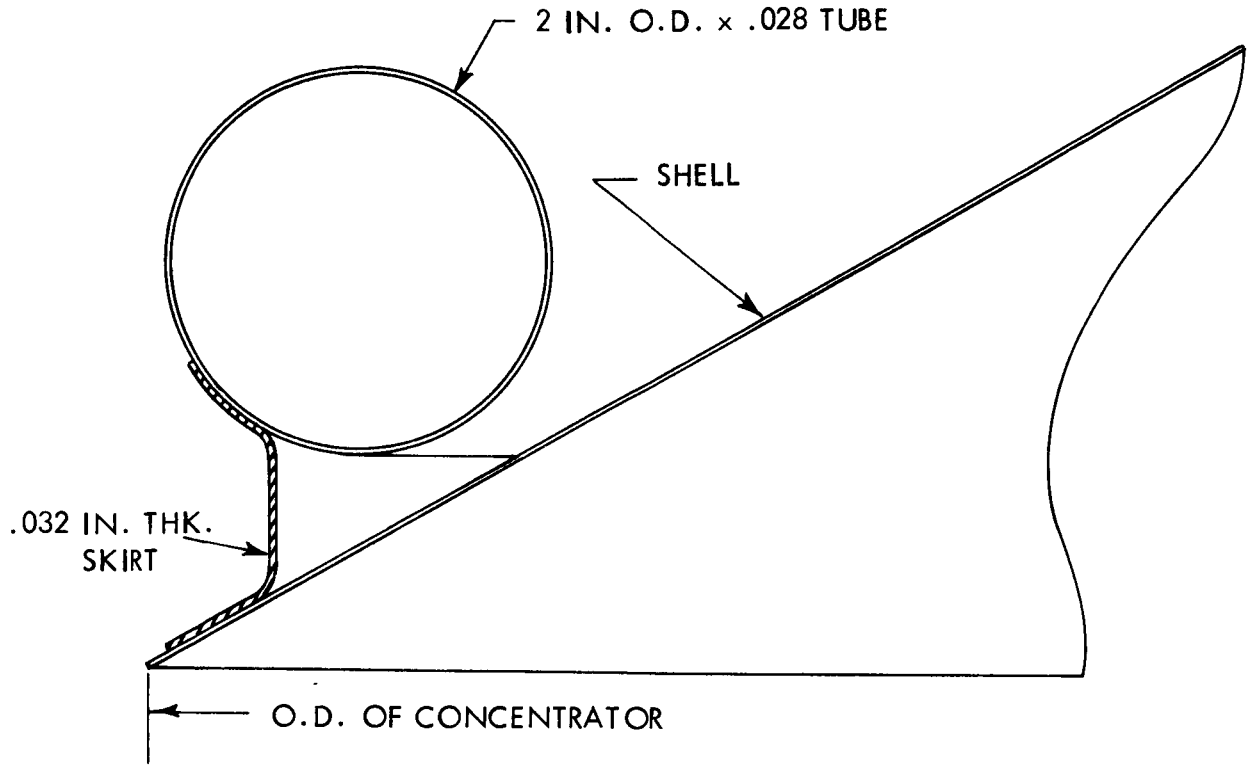

FIGURE 12a
TUBE TORUS AND SKIRT DESIGN

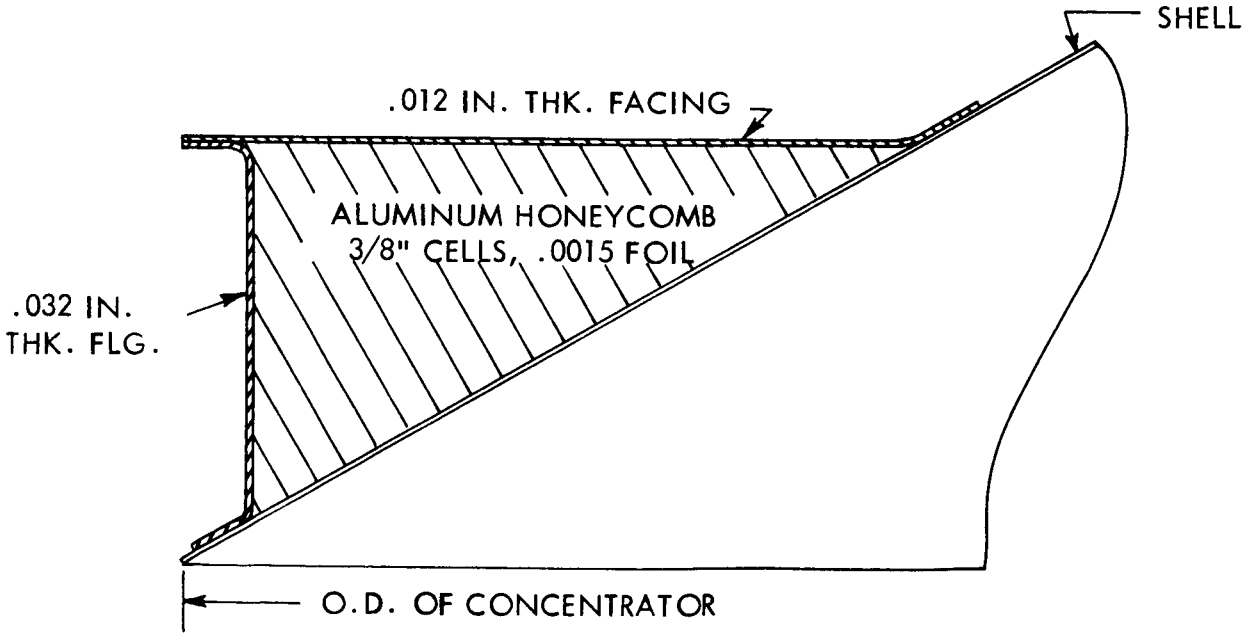

FIGURE 12b
BUILT-UP TRIANGULAR RING DESIGN

FIGURE 12
MOUNTING RING DESIGN

(ref. 4). A distributed torque of magnitude $T = 1.5(N_\phi) = .98$ inch pounds per inch acts on the ring. Every section of the ring is subjected to a bending moment $M = TR$ which results in stresses (see figure 11 for nomenclature)

$$\sigma = \frac{Mr}{I} = \frac{TR_r}{\pi hr^3} = 320 \text{ psi}$$

A torus on three supports when loaded normal to its plane of curvature will act like a curved beam and will experience both moment and torsion. If the torus is not fixed as to roll, the maximum moment is,

$$M = w R^2 \frac{\sin\frac{1}{2}\theta - \frac{1}{2}\theta \cos\frac{1}{2}\theta}{\sin\frac{1}{2}\theta}$$

where θ = 120 degrees for 3 supports

$w = W + N_\phi \sin\phi = .33 + .33 = .66$ lb per inch

W = inertial load of the ring itself

The maximum moment which occurs over the supports is

$$M = .396\, w R^2$$

or $M = 220$ in-lb

The resultant bending stress is 2500 psi. The twisting moments will be a maximum approximately 26 degrees from the support. The maximum twisting moment is 47 inch pounds which results in a shearing stress of 270 psi.

With the ends of the 120 degree ring segment fixed from radial movement, the component of shell edge force in the plane of the ring will result in end forces and moment in the plane of the ring. Due to the redundant moment, the ring stress will equal 300 psi for the $N_\phi \cos\phi$ loading of 0.57 pounds per inch.

The absolute maximum stress in the tube torus would require an examination of location as well as orientation of the stresses thus far indicated. The absolute maximum stress will not be greater than 3000 psi; it occurs in the vicinity of the support and is due primarily to out-of-plane ring bending from axial components of the 10 G load.

The skirt for the tube torus design was sized by considering it to be a short cylinder under a uniform radial shear equal to the $N_\phi \cos\phi$ loading of 0.57 pounds per inch. Case 10, Table XIII and p. 277 of Roark (ref. 4) provide the correct formulas to calculate radial displacement and maximum moment and stress. A cylindrical skirt of 29.5 inch radius, of 1 inch length, and of .032 inch thickness will deflect .006 inches and will experience 800 psi bending stress due to the maximum moment that develops nearly two-thirds of the distance from the free loaded end.

The fasteners or fixtures for mounting the assembly have been designed

as female threaded fasteners and they take the form of two cylindrical plugs welded into the ring cross section at each attachment location. The equation

$$\sigma_{max} = \frac{P}{2t^2} \log_e \frac{0.3r}{b}$$

from Roark (ref. 4), page 283, might be used to guide the design where P equals the total inertia load divided by 12 as there are 3 mounting fixtures with the load going into each distributed over 4 concentrated areas of the ring. The radius of the load area is b.

The equation indicates that the stress will be a minimum if the ratio of r/b is chosen correctly. This led to the selection of 5/8 inch diameter plugs for the 2 inch diameter tube.

Honeycomb stiffened triangular ring analysis. -The triangular ring shown in figure 12b was sized to weigh the same as the tube-torus-skirt design. This comparable weight approach was considered most useful in evaluating the results of the strain gage static load tests. Note that the outer flange or cylindrical skirt of the triangular ring is .032 inch thick or nearly 3 times the thickness of the .012 inch thick flat sheet closing out the section. The honeycomb sandwich cells run more nearly normal to the thin face and will, therefore, stabilize this face; they will not, however, provide much resistance to instability of the outer flange and this sheet must,therefore, be heavier.

Fasteners molded into the honeycomb core were used as mounting fixtures. Two were used at each support location located 2 inches on center as with the welded inserts in the tube torus design.

Sample Ring Fabrication

Tube-torus-skirt design. -TRW's vendor experienced difficulty in rolling the 5 foot diameter torus out of the 2 inch by .028 inch thick tube stock. A sand fill only was used to internally support the tube during rolling with the result that very deep wrinkles developed along the inner circumference of the torus. Ultimately a satisfactory but not perfect ring was rolled from 6061-T4 aluminum in .035 inch thickness. This ring was used for the partial ring tests and evaluation.

Flatness and overall diameter tolerances of ±1/16 inch were nearly met by the vendor. As expected, the tube cross section was out of round---as much as 0.30 inch difference in the in-plane and out-of-plane diameters---and wrinkles were still noticeable along the inner circumference.

No difficulty was experienced in welding the mounting fixture inserts into the .035 inch thick tube.

The skirt was slotted so that it could be developed into a cylinder. After fitting the skirt to both the torus and the shell panel, it was bonded to the torus and then, a day later, it was bonded to the panel. Glass cloth was used between the parts to insure a nearly uniform adhesive thickness. The as fabricated cross section is shown as Figure 13a.

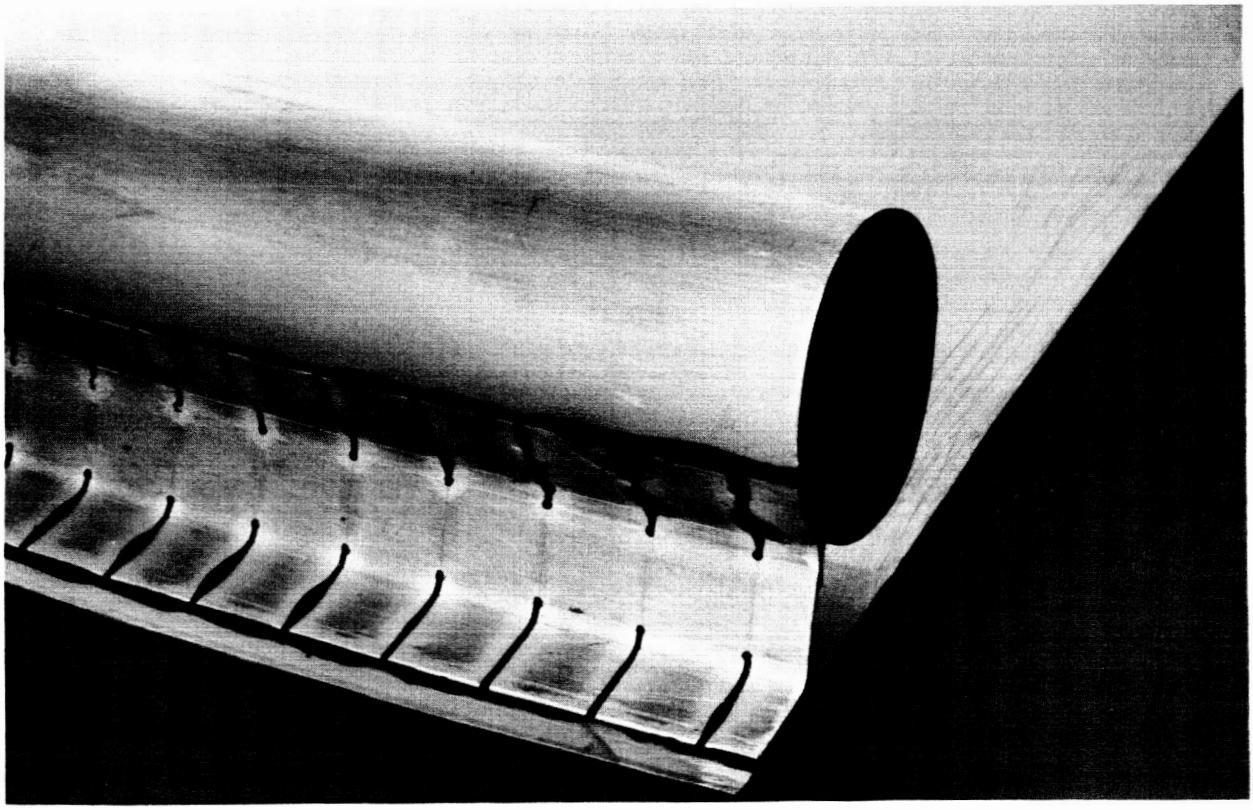

FIGURE 13a

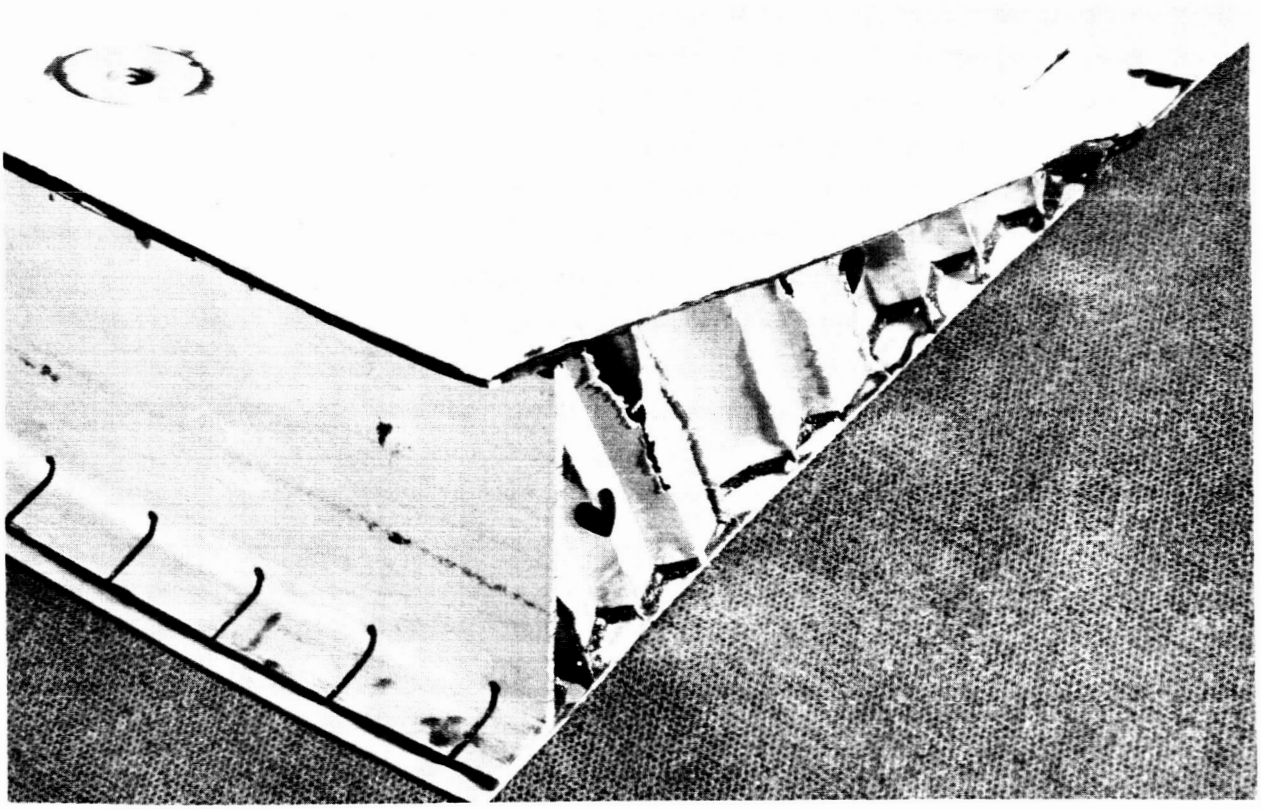

FIGURE 13b
MOUNTING RING HARDWARE

Honeycomb stiffened triangular ring fabrication. -It was the original intention to run the honeycomb cell direction normal to the flat sheet or back of the triangular ring. As the honeycomb was machined in the unexpanded form, this resulted in an unacceptable stepped surface along the face that would bond with the stretch formed panel. To achieve a better fit so as to minimize markoff, the honeycomb cells were oriented normal to the back of the reflector surface. It was also necessary to allow for the effect of honeycomb ribbon direction contraction as the core is expanded. After a few trial machining efforts, an excellent final cross section was achieved.

The outer flange or skirt was slotted and fitted much in the same way as the skirt for the tube torus. No difficulty was encountered in bonding the assembly together. No glass cloth was used at the core and concentrator panel interface; to make this bond, the core was adhesive dipped to minimize both the weight and the mark-off to the reflective surface of the concentrator. Figure 13b shows the fabricated section including one of the molded-in fasteners.

Test and Evaluation of Sample Rings

Test purpose and description. -The sample rings were tested and evaluated as an aid to final design of a support ring for a 60 inch diameter solar concentrator. The bases for evaluation are: (1) minimum degradation of the shell reflective face as a result of attaching the support ring and (2) optimum structural efficiency of the ring and fixtures including specifically the static load capacity of the mounting fixture.

The projected grid optical method was used to determine the comparative surface quality of the shell face in the vicinity of the support ring. The ring is bonded to the panel and, then, prior to any structural testing, the panel is optically inspected. A description of the optical inspection rig will be presented in a later section.

While only a single stretch of 25 inch wide stock is used for each of these tests, the continuity of the ring is maintained. It was easier to do this than to fixture and restrain a partial ring so that deflection behavior under load approximates that of a complete torus. Figure 14 shows the typical test setup with the panel under test. One mounting fixture is centered at the one panel edge with the other fixtures equally spaced 120 degrees around the ring. Strain gages were mounted along the centerline of the panel in the vicinity of the ring-shell junction. Gages were mounted both front and back of the panel and at both the fixtured and non-fixtured end of the panel.

The test described briefly here is then repeated with a second stretch formed panel and the alternate ring cross section. In this case the triangular ring was terminated about 8 inches beyond the test panel. Ring continuity was achieved by bonding the ends into segments of the now discarded tube torus from the first test.

As a final test of the ring and mounting fixture arrangement, sections of both test rings which contained the fastener inserts were cut out of the assembly and loaded to failure in a standard tensile testing machine.

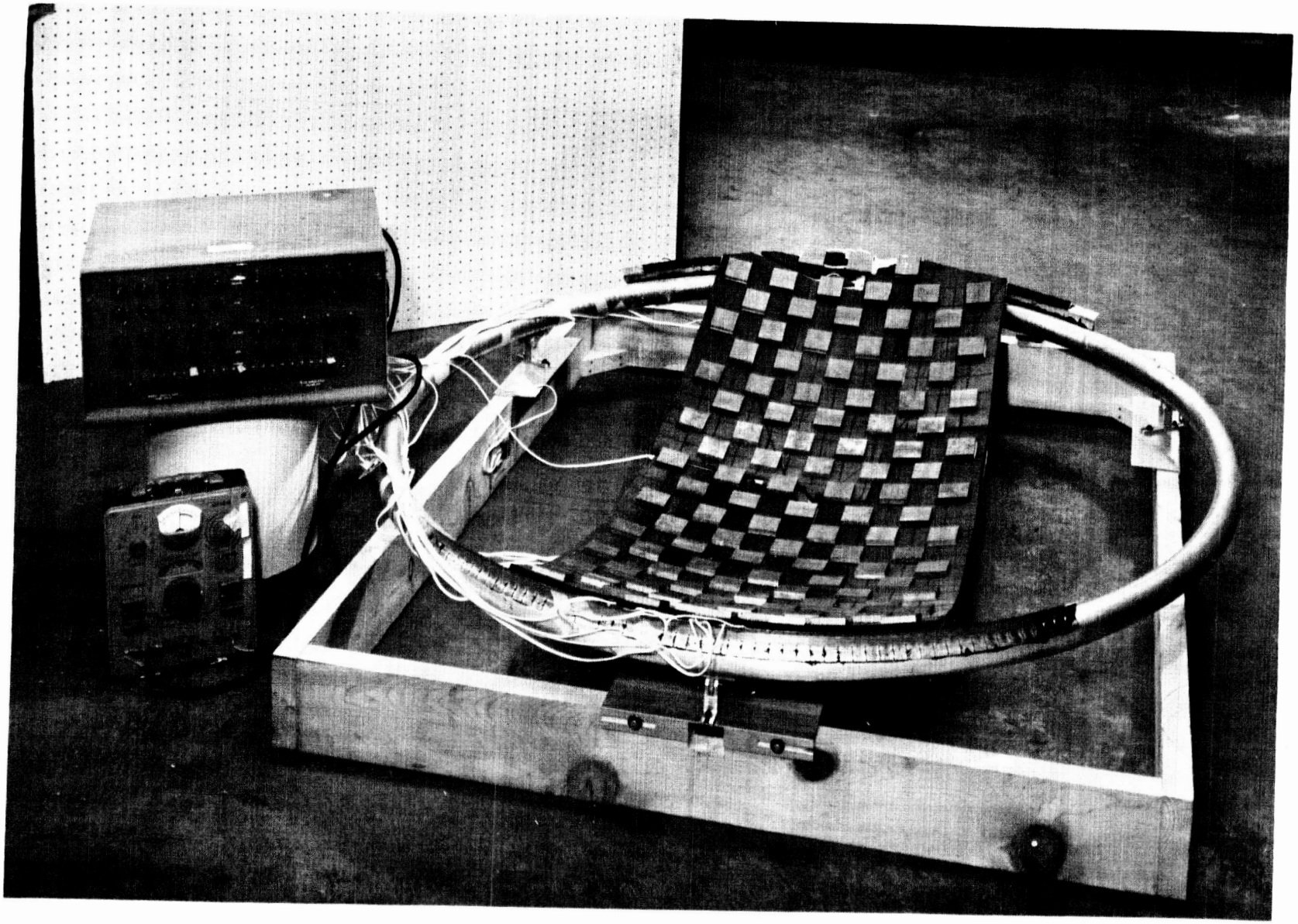

FIGURE 14
MOUNTING RING TEST ARRANGEMENT

Further details of the instrumentation and test procedure will be described in the paragraphs to follow.

Support ring mark-off to shell reflective face. -Full scale photographs of the reflected grid shadow and pattern in the vicinity of the ring were made for each of the two test panels and ring assemblies. During inspection, the assemblies were supported at the mounting fixtures without the aid of the glass master.

Figures 15 and 16 are representative inspection photographs of each of the ring-shell assemblies. Close examination of the two photographs will indicate that the deviations of the grid shadow from the pattern and, hence, the distortions are greater for the triangular ring assembly than for the tube-torus design.

Representative zones of the several inspection photographs were evaluated on a point-by-point basis. Data from the better half of each test assembly are shown in figures 17 and 18. Comparative values of distortion are presented as a function of distance from the concentrator rim. The curves were developed by plotting average values of distortion for each one inch increment of radial distance.

In figure 18, note that after an initial high value of distortion an angular error of 4 minutes remains until after the end of the honeycomb built-up section is reached (about 4.5 inches from the rim). The tube-torus design, on the other hand, did not exhibit as high an edge distortion and, additionally, attenuates continuously to a nominal 2-minute error.

The poorer half of the built-up triangular ring supported panel exhibited distortions that were larger than those shown in figure 18. This was particularly true near the inner tabs of the built-up ring (4 inches in from the ring) where the average distortions were more than twice as high as the 4-minute errors indicated in figure 18. This has been attributed to extra adhesive that was paddled on the tabs during the lay-up.

The panel load test evaluation. -Electrical strain gages were installed in the region of the ring-shell junction of both ring-shell assemblies. Instrumentation (see figure 14) consisted of a twenty channel switch and balance unit into which the active gages and a common temperature compensating "dummy" gage were wired and an SR-4 single channel indicator.

Deadweight loading into the face of the concentrator panel was applied with 2 x 2 x 3/8 inch steel blocks. A 3/8 inch thick foam rubber pad was placed between the panel and the load blocks to distribute the load. A grid was laid out on the pad to aid in the placement of the blocks; by changing the placement and number of blocks, several equal load levels could be applied to each of the test panels.

The results presented here are in terms of a 0.02 psi surface loading equivalent to a 6.0 lb concentrator in a 10 G acceleration field. Stresses were computed from strains using the standard biaxial stress-strain relations which are appropriate for the panel centerline or line of symmetry.

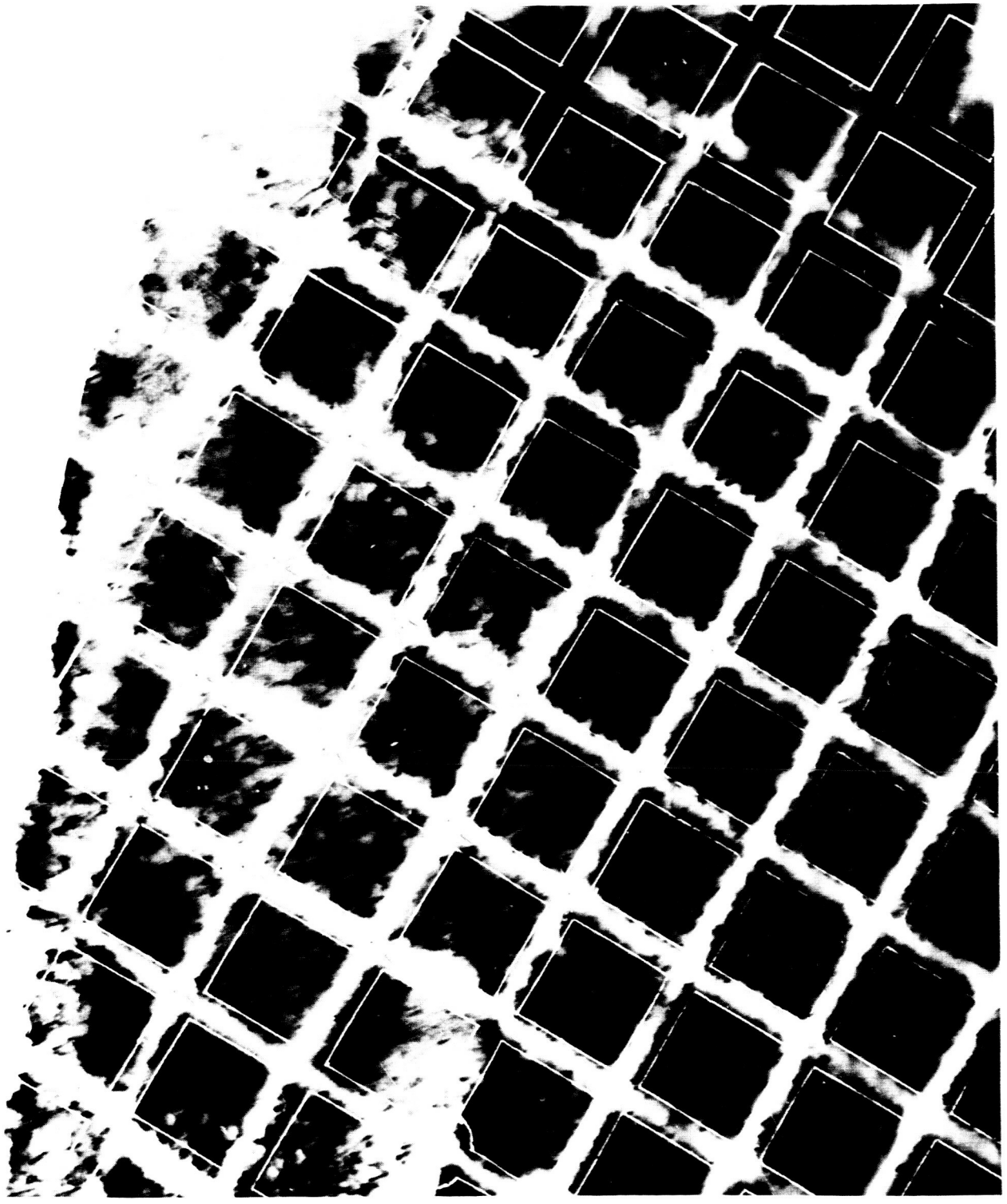

FIGURE 15
TUBE-TORUS & SKIRT OPTICAL INSPECTION

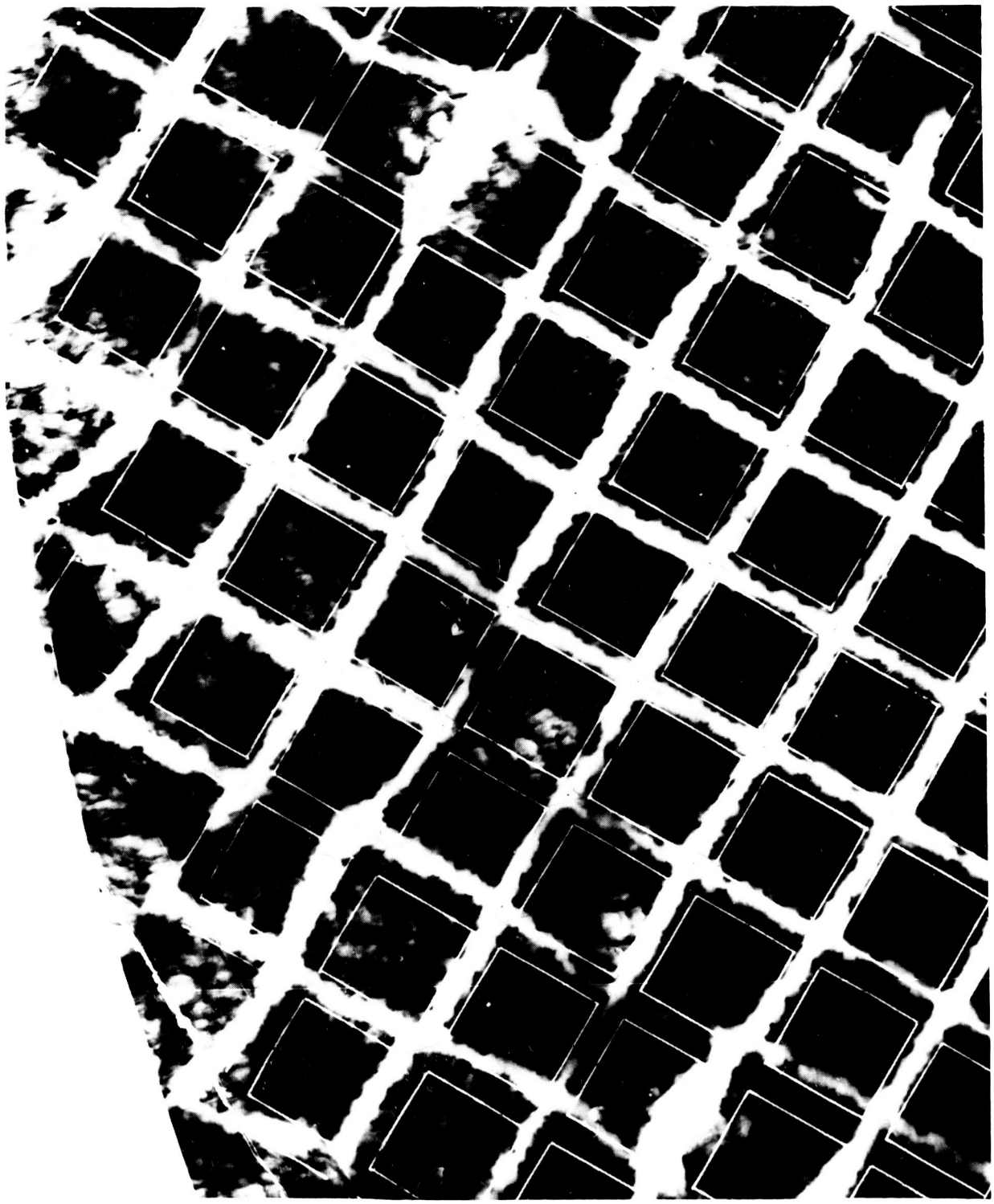

FIGURE 16
TRIANGULAR RING OPTICAL INSPECTION

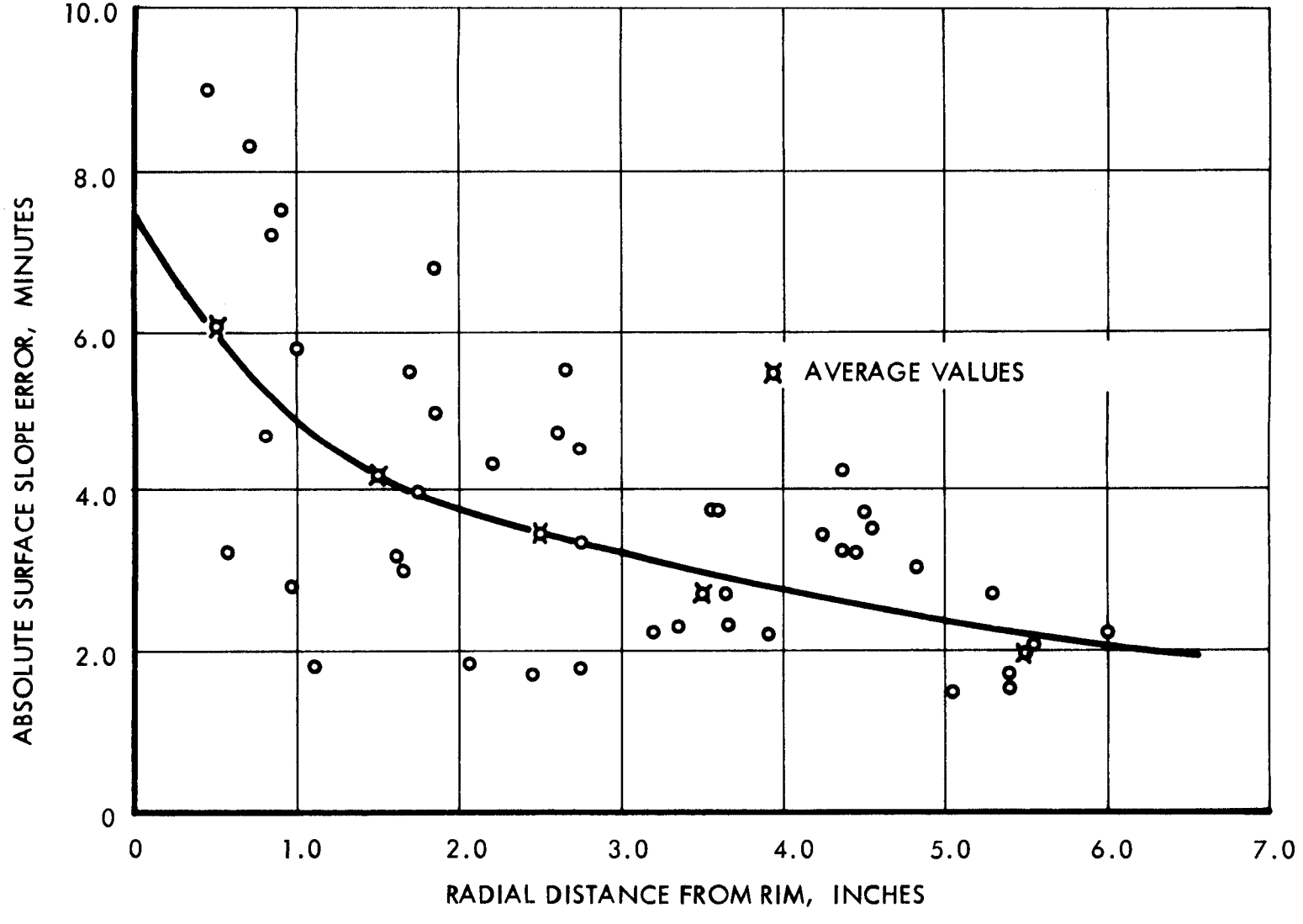

FIGURE 17
TUBE AND SKIRT TORUS OPTICAL INSPECTION DATA

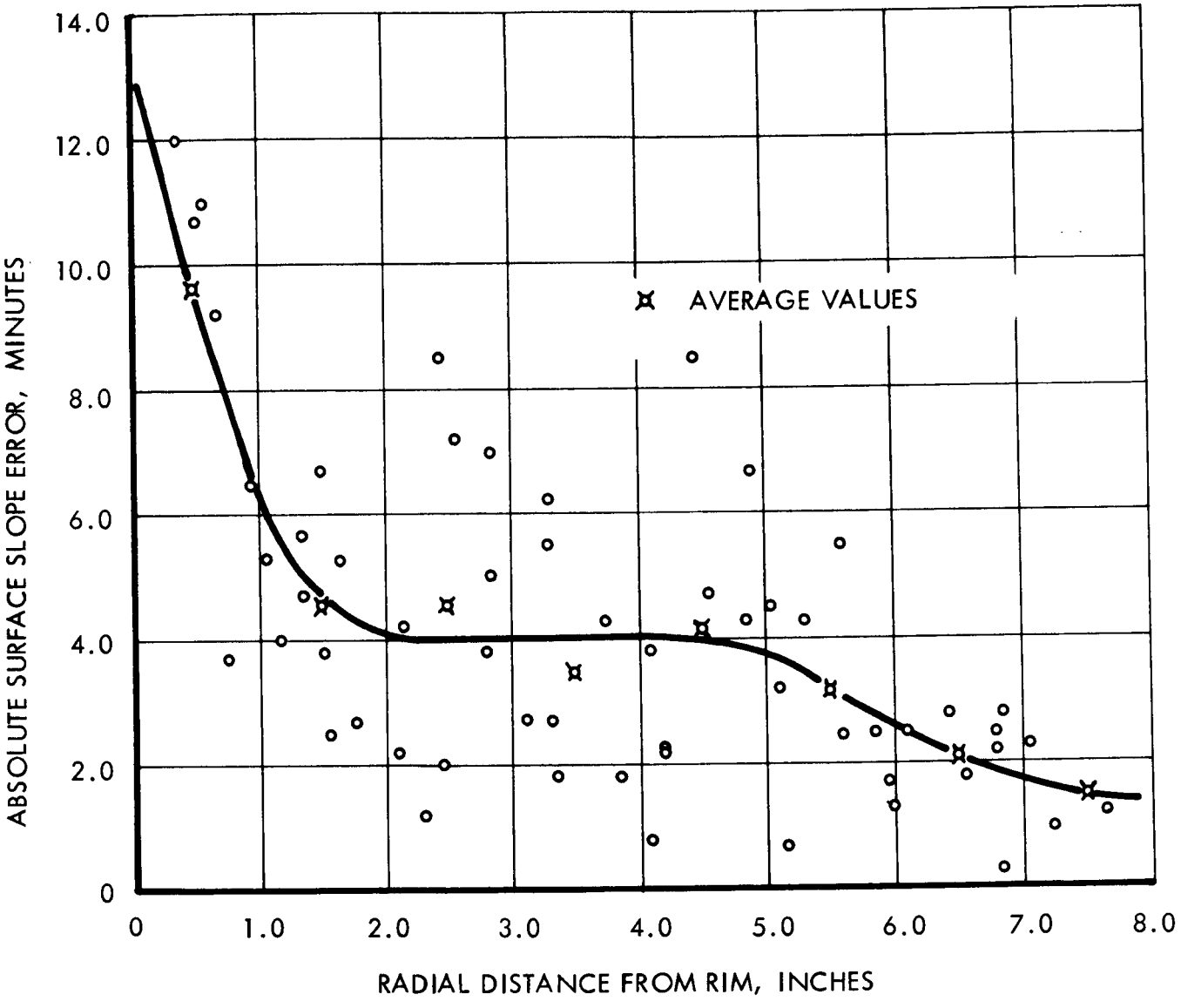

FIGURE 18
TRIANGULAR RING OPTICAL INSPECTION DATA

For the tube torus, the maximum meridional stress was 1600 psi and for the triangular ring about 1100 psi. These values are based on strains measured closest to the ring-shell junction (the gage centerline was .250 inch from the end of the support ring skirt attachment). If the maximum front or back stresses (both radial and circumferential at both the fixtured and non-fixtured end) are averaged, the tube torus design experiences stresses about twice those measured for the triangular ring design. Therefore, one can conclude that the triangular ring design is somewhere between 1.5 (the ratio of 1600 to 1100) to 2.0 times as efficient as the tube torus skirt design in getting inertia loads out of the shell without distorting or producing high stresses at the ring-shell junction.

The maximum stresses are primarily a result of high bending in the region of the ring-shell junction. With gages on both the front and back of the panel, it was possible, of course, to separate the uniform membrane component of stress from the bending component. If the calculated meridional membrane stress

$$\sigma_{\phi} = \frac{N_{\phi}}{t} = \frac{.65}{.016} = 40 \text{ psi}$$

is compared to the total maximum stress measured (1600 psi) the ratio of measured discontinuity stress to calculated membrane stress is 40 and could even be larger at the joint itself.

Based upon the measured stress levels, it is seen that the tube-torus-skirt design provides a factor of safety over the maximum acceleration of 10 G's to account for other environmental loads. Limiting the stress in the shell panel to 6000 psi (this is conservative since the yield strength will increase due to work hardening during stretch forming) the panel could accept nearly 40 G's before any yielding will occur.

The measured surface stresses can be related to a bending moment at the ring-shell junction. For front and back stresses of ±1600 psi the equivalent moment in the .016 inch thick stock is .068 in-lb per inch. This can be thought of as a peel moment or requirement imposed on the adhesive.

No great differences in maximum stress were measured at either the fixtured or non-fixtured end of the panel or as a function of the type of loading. Generally, the maximum stresses would fall somewhere between 1000 psi and the indicated 1600 psi. The sign of the stress may change or the direction (circumferential rather than radial) depending on the test condition. To relate any one specific stress value to an analytically determined value would require a redundant force and moment analysis taking into consideration the deflection and rotational behavior of the shell and ring under the exact loading and support conditions.

Tensile test of mounting fixtures. -An 8-inch section of tube that included the welded-in inserts was cut from the tube torus and epoxy molded into a tensile test fixture (see figure 19a). The clear span between the support blocks was 5.0 inches. Loaded in tension, yielding began at 625 pounds not in the tube but in the mounting lug that spanned the 2.0 inch center to center of the inserts. The lugs, of 6061-T6 aluminum, had been sized assuming a 600 pound

load and yield at 35,000 psi. The test was terminated at a load of 1500 pounds with no visible damage or deflection to the 2.00 inch x .035 tube or the welded-in inserts. The fixtures were, therefore, overdesigned in that 10 G acceleration on a 12 pound concentrator would be equivalent to only 40 pounds load per mounting fixture.

The comparable test piece and loading fixture for the triangular ring and molded-in fasterners is shown in figure 19b. Again the spacing between supports was 5.0 inches. Slight non-linearity of load to deflection was apparent at a load of 275 pounds with little yielding until about 400 pounds. The ultimate capacity was 500 pounds with the primary mode of failure being the .012 inch face separation from the core.

Final Mounting Ring Design

The final design of the five-foot diameter stretch formed solar concentrator is shown in figure 20. The support ring design is similar to the tube torus and skirt sample that was tested and evaluated. Mounting fixtures take the form of a single insert welded into the tube at three locations.

The considerations that resulted in the selection of this design are as follows:

(1) Surface errors from ring mark-off were smaller for the tube torus and skirt design than for the triangular ring section. Improvement in surface quality is possible with either design; nevertheless, the likelihood of a high quality surface is best if the contact area of the ring at the shell is minimized consistent with other requirements. The honeycomb of the triangular ring did not appear to markoff; however the bonding of tabs 4 inches in from the concentrator rim will tend to affect more surface area at the higher distortion level.

(2) The tube torus and skirt is a satisfactory structural concept for the imposed environment. The final design uses a 1.75 inch OD by .035 inch tube with only 3500 psi stresses at 10 G. Thus, aluminum alloy 6061 which has a yield of 5000 psi in the soft condition satisfies the 10 G strength requirements. In addition, the tube will work harden during rolling which has the effect of increasing the material yield.

Based on the strain gage tests, the triangular ring is better able to prevent the build-up of stresses at the ring-shell junction than the tube and skirt torus. Nevertheless, either design is more than adequate for the intended load application. For the 3003-0 aluminum with a 6000 psi yield, the panel could withstand 37.5 G's if maximum stresses at the ring-junction are 1600 psi for 10 G acceleration. Again, the strain hardening introduced during stretch forming will allow higher loadings.

(3) The strength of the welded-in mounting fixture is high. The molded-in fasteners would have been adequate for the intended application, but the more than 1500 pound capacity of the two welded-in inserts leads to the selection of a single welded-in insert for the final design.

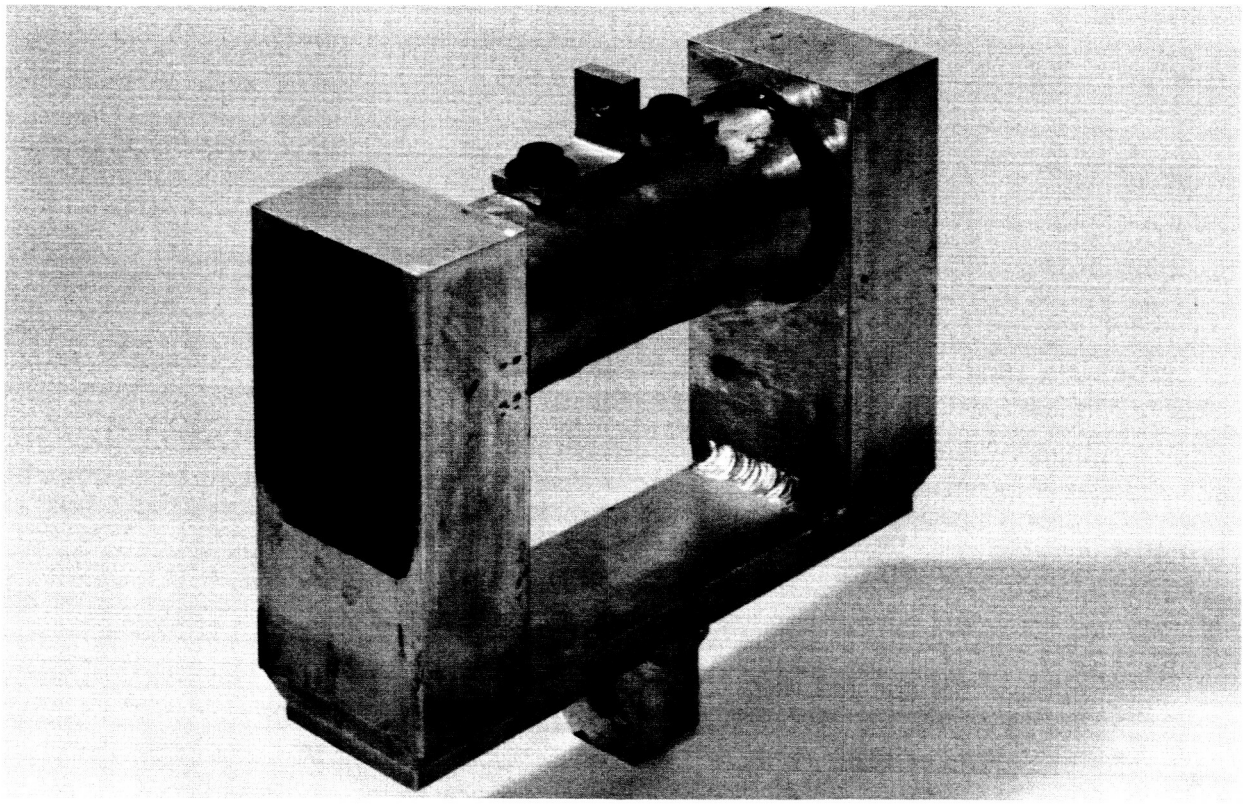

FIGURE 19a

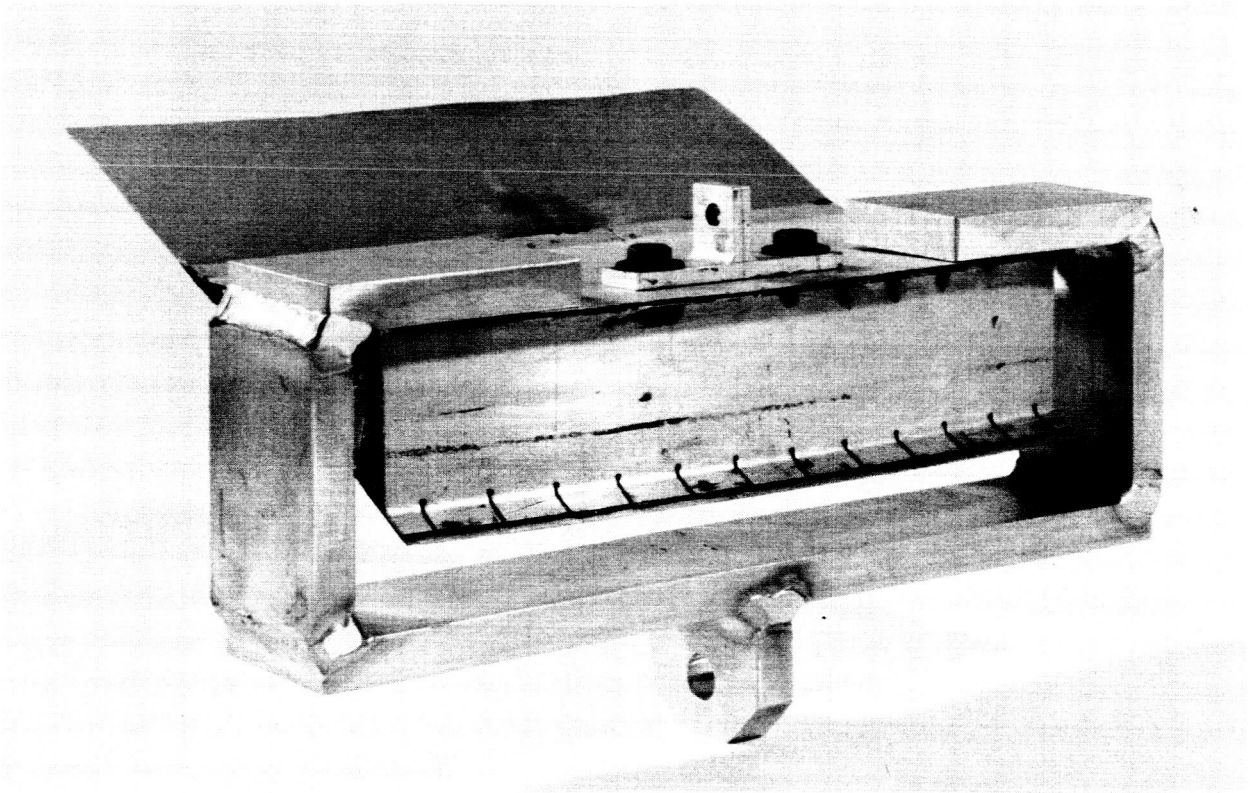

FIGURE 19b
MOUNTING FIXTURE TENSILE TEST SPECIMENS

CONCENTRATOR FABRICATION

The final concentrator design as shown in figure 20 consists of a stretch formed 60 degree rim angle paraboloidal reflector composed of 8 segments bonded together with radial splices. The support ring design is a tube torus and skirt which is adhesive bonded to the back of the reflector shell. This design configuration utilizes the previously discussed research and development investigation results.

The fabrication process which was also finalized during this investigation is presented in Appendix A. The critical cleanliness operations of stretch forming, surface improvement coating, final assembly, and optical inspection are conducted in one area so that the cleanliness conditions can be controlled. A layout of this area showing the alternate positions of the master parabolic tool and the filtered air units is presented in figure 21.

The concentrator fabrication portion of the contract consisted of putting the research and development investigation results into practice on a multipart basis. These efforts will now be discussed for the major fabrication operations.

Stretch Forming

Ten sheets were stretch formed - from which the final hardware could be selected. This resulted in twenty sector panels when the full sheets were cut in half. Stretch formed panel quality improved and became more consistent as stretching progressed. The major blemish which would reject a panel is the dimpling effect caused by lube pile-up due to nonuniform lube or dust. From the 20 panels, 4 were rejected due to excessive dimpling and 2 were scrapped due to handling damage.

Surface Improvement Coating

The 14 remaining panels were spray coated and cured as described in Appendix A. Again, the repetition of spraying many parts improved the general quality. However, it was found that the necessity of readjusting the spray gun directions and spray pattern after each spray (as required because of cleaning to prevent inclusion blemishes) limited the repeatibility of the spraying operation.

A medium to fine orange peel was present on all panels and the surfaces showed only the occasional occurrence of dust and entrapped particles. The most obvious blemishes (which were noted on all parts) are the previously discussed "pin holes" or crators.

Of the 14 panels which were spray coated, 3 were scrapped. One was rejected due to runs in the coating, one due to handling damage, and one due to surface cracking from improper curing.

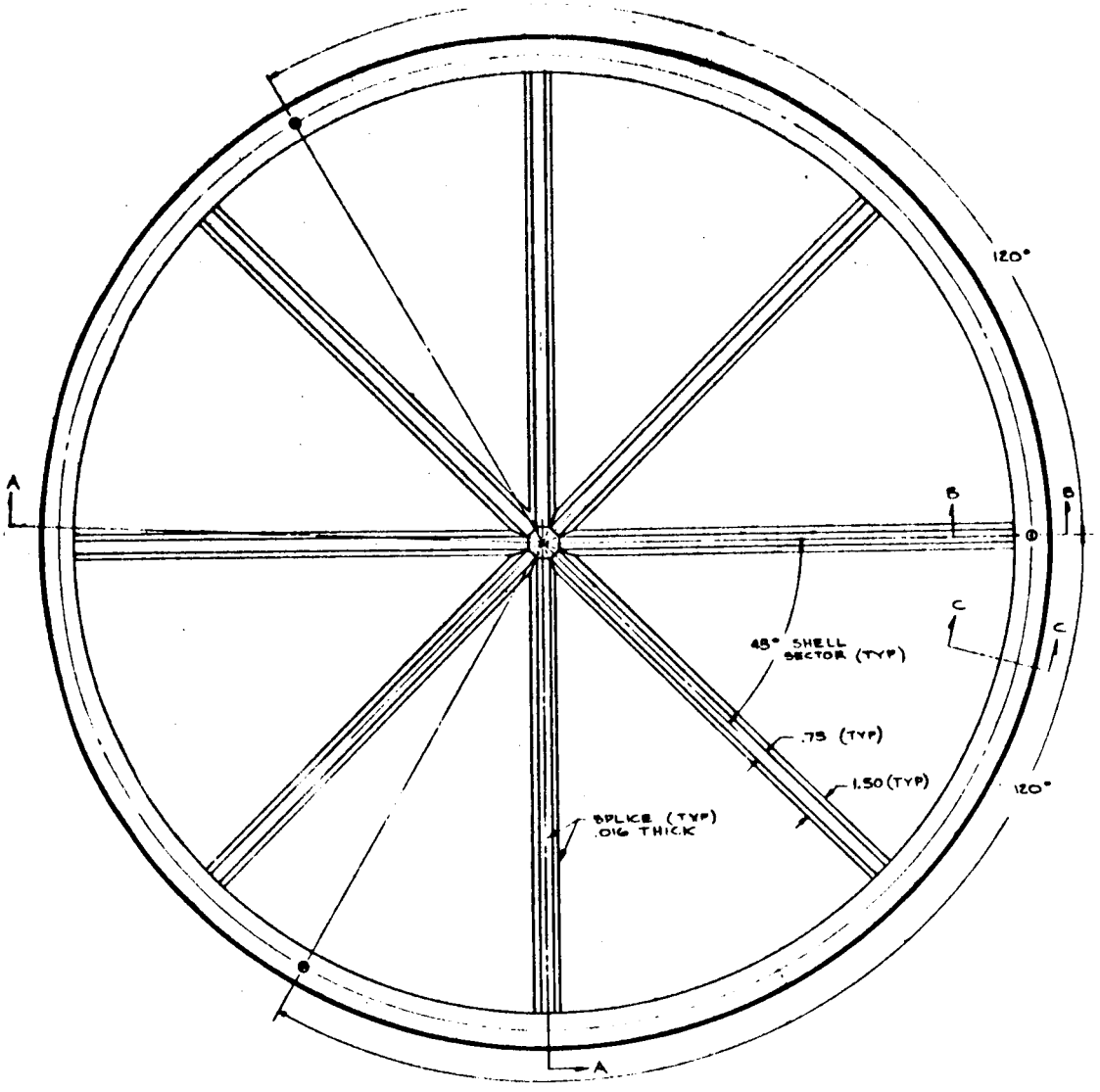
120°
A
B
B
C
C
45° SHELL SECTOR (TYP)
.75 (TYP)
1.50 (TYP)
SPLICE (TYP) .016 THICK
120°
A

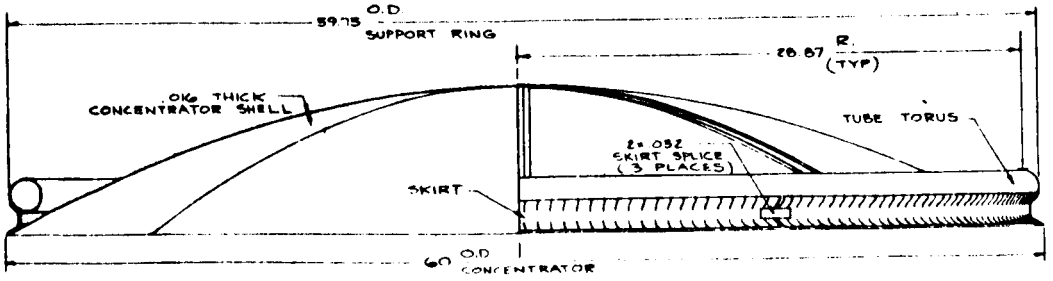
59.75 O.D SUPPORT RING
28.87 R. (TYP)
.016 THICK CONCENTRATOR SHELL
TUBE TORUS
2 .092 SKIRT SPLICE (3 PLACES)
SKIRT
60 O.D CONCENTRATOR

VIEW A A

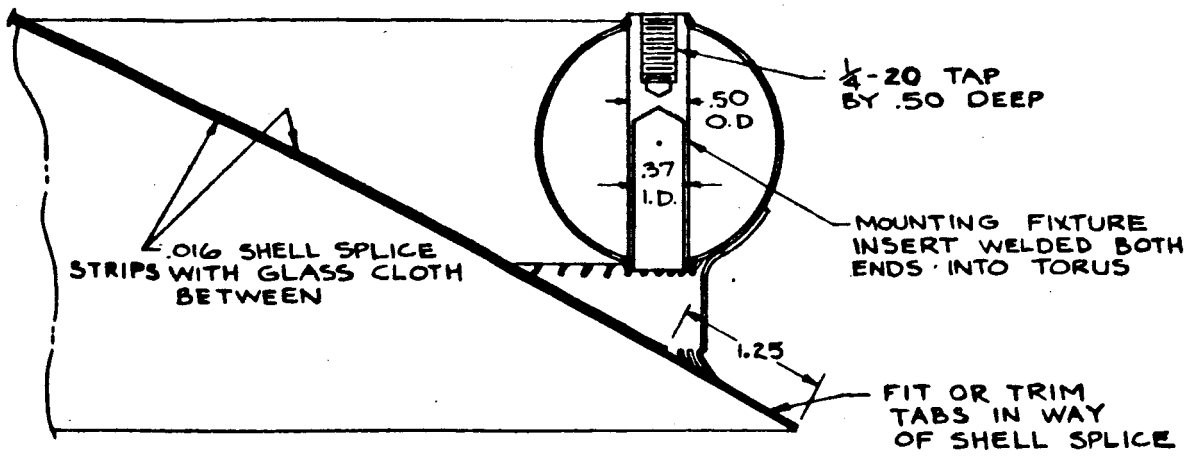

SECTION B-B
THROUGH SPLICE & MOUNTING FIXTURE

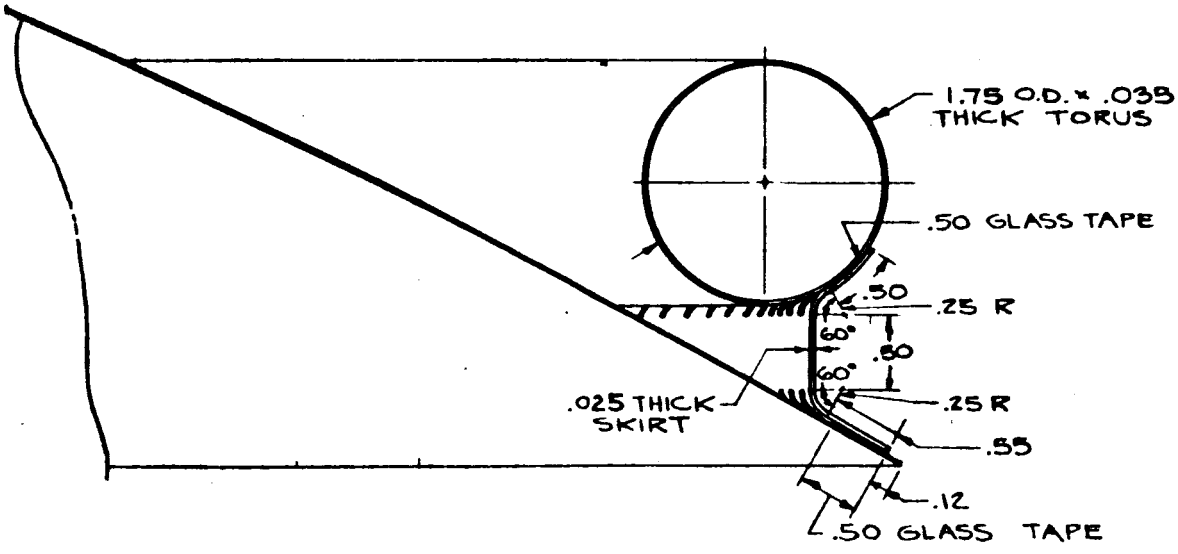

SECTION C-C
THROUGH CONCENTRATOR SHELL

FIGURE 20
FINAL CONCENTRATOR DESIGN

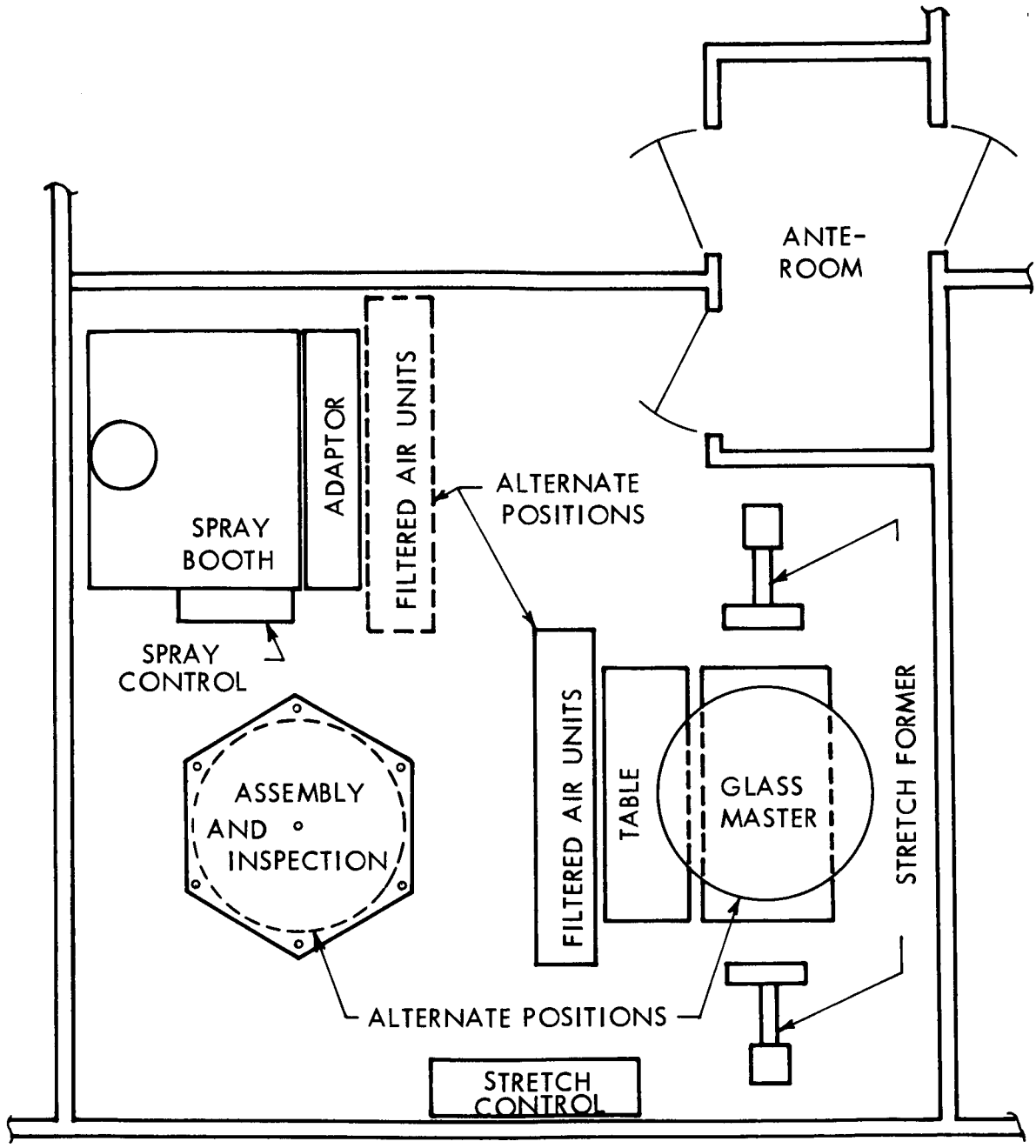

FIGURE 21
FABRICATION FACILITY LAYOUT

Aluminizing, Trimming and Inspection

The remaining 11 panels were aluminized in the vacuum coating facilities available at TRW. The vacuum tank is 16.5 feet long and 5 feet in diameter and has the capability to deposit both dielectric and metal films. Also, glow discharge substrate cleaning is available. For a further description of this facility see reference 5. The mirroring process consists of the vacuum deposition of a thin film of silicon oxide onto the epoxy surface improvement coating to act as a tough sealing and adhesion layer. On this layer, the high purity aluminum film is vacuum deposited to obtain a high reflectivity.

The aluminized panels are then cut to the proper sector shape using the trimming saw arrangement previously described. The range of edge distortions which were experienced has been presented in figure 8. The wide variation of distortion is due to the lack of process control in the feed and pressure of advancing the slitting saw.

After trimming, the sectors were placed on the glass master in the optical inspection rig and grid inspection photographs were obtained through the transparent glass master.

From the 11 panels, 8 were selected for the final concentrator assembly based upon geometric quality, epoxy coating characteristics, edge distortion condition, and reflectivity.

Final Assembly

The final assembly is made on the glass master parabolic tool while in position on the optical inspection rig. (refer to figure 21) In this way, the optical characteristics of the assembly, as it progresses, can be continuously observed. The final assembly consists of two major subassemblies - the mirror shell, and the support ring.

The mirror shell assembly is composed of the 8 sectors bonded together by radial splice strips. The support ring assembly is then bonded to the shell to provide the final structural configuration. The mirror shell was held in intimate contact with the master tool during the assembly operation by pulling a vacuum between the panels and the tool.

Final Inspection

The completed mirror is now structurally rigid and can be supported by the mounting ring through the three mounting fixture points. The glass master is parted from stretch formed concentrator and removed from the inspection rig.

The 60 inch concentrator is shown in the optical inspection setup in figure 22. This arrangement utilizes the optical characteristics of a paraboloid to detect any gross deviations from a true parabolic surface.

FIGURE 22
OPTICAL INSPECTION ARRANGEMENT

Located at the focal point is a small light source which illuminates the concentrator. The reflected light from the mirror is nominally parallel to the optic axis by virtue of the optical characteristics of a paraboloid. By viewing the grid-screen arrangement which is aligned to be parallel, deviations of the reflecting surface are observed as misalignment of the grid shadow on the screen. Since the screen in this arrangement is a plexiglass sheet with the grid pattern outline on it, rapid inspection and a permanent record is made by placing photographic paper underneath the plexiglass for short period exposure while the room is completely darkened except for the point light source at the focus. Thus a full size photograph (60 inches in diameter) is obtained of the mirror. A composite of the inspection photographs for the 60-inch concentrator is shown in figure 23. Since exposure sensitive photographic paper is used, the inspection photographs are actually negatives with the dark areas representing the reflected light passing through the grid.

Each grid increment represents an inspection data point for which a specific surface deviation is obtained from the inspection photograph by measuring the mismatch of the grid shadow (white heavy lines) with respect to the grid pattern on the screen (white fine lines). The proportionality of the surface rotation to the mismatch is calculated from the geometric relationship of the grid and screen.

The geometric quality of the 60-inch concentrator as measured by this method will be discussed in the next section.

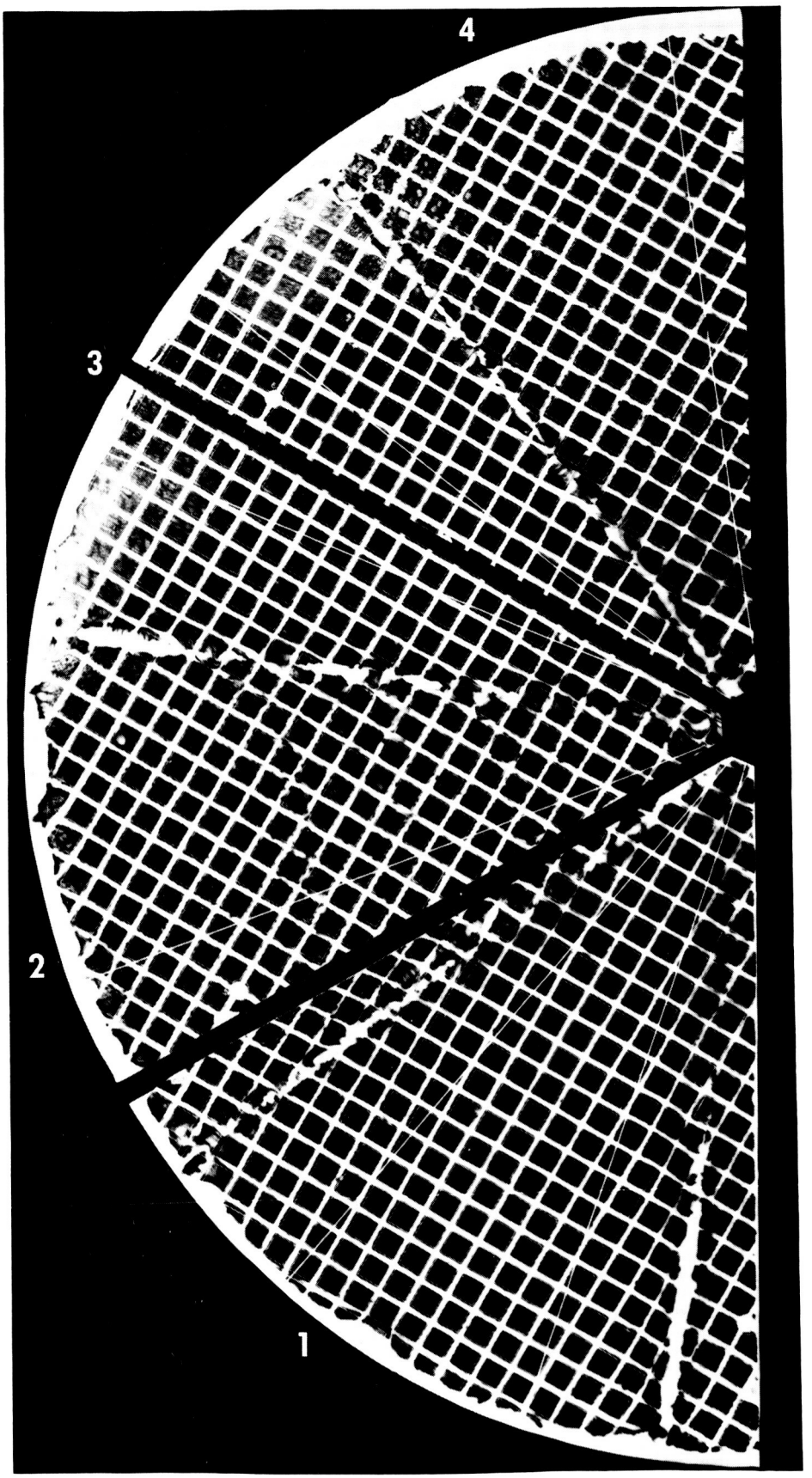

FIGURE 23

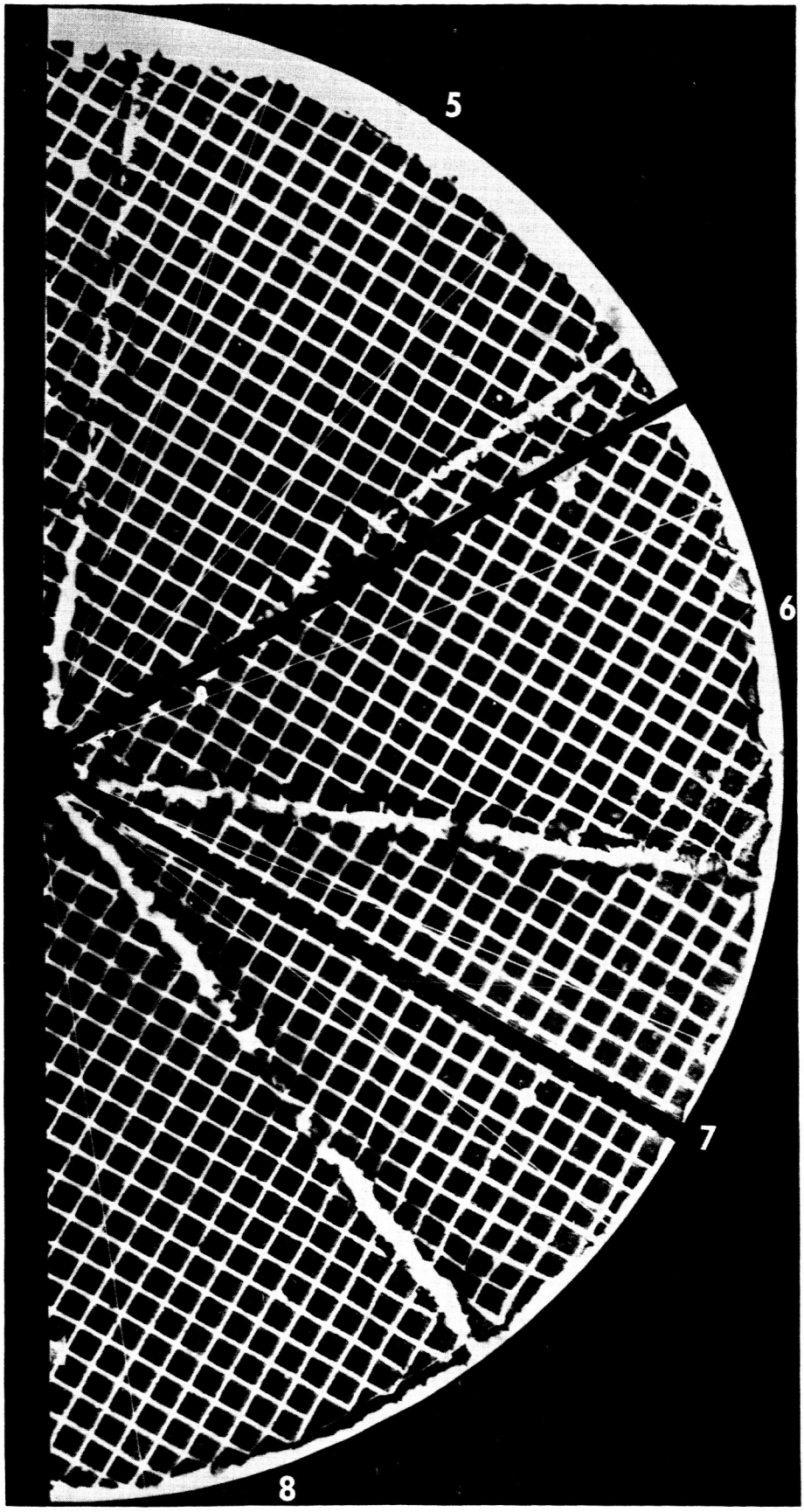

FIGURE 23
INSPECTION PHOTOGRAPH COMPOSITE

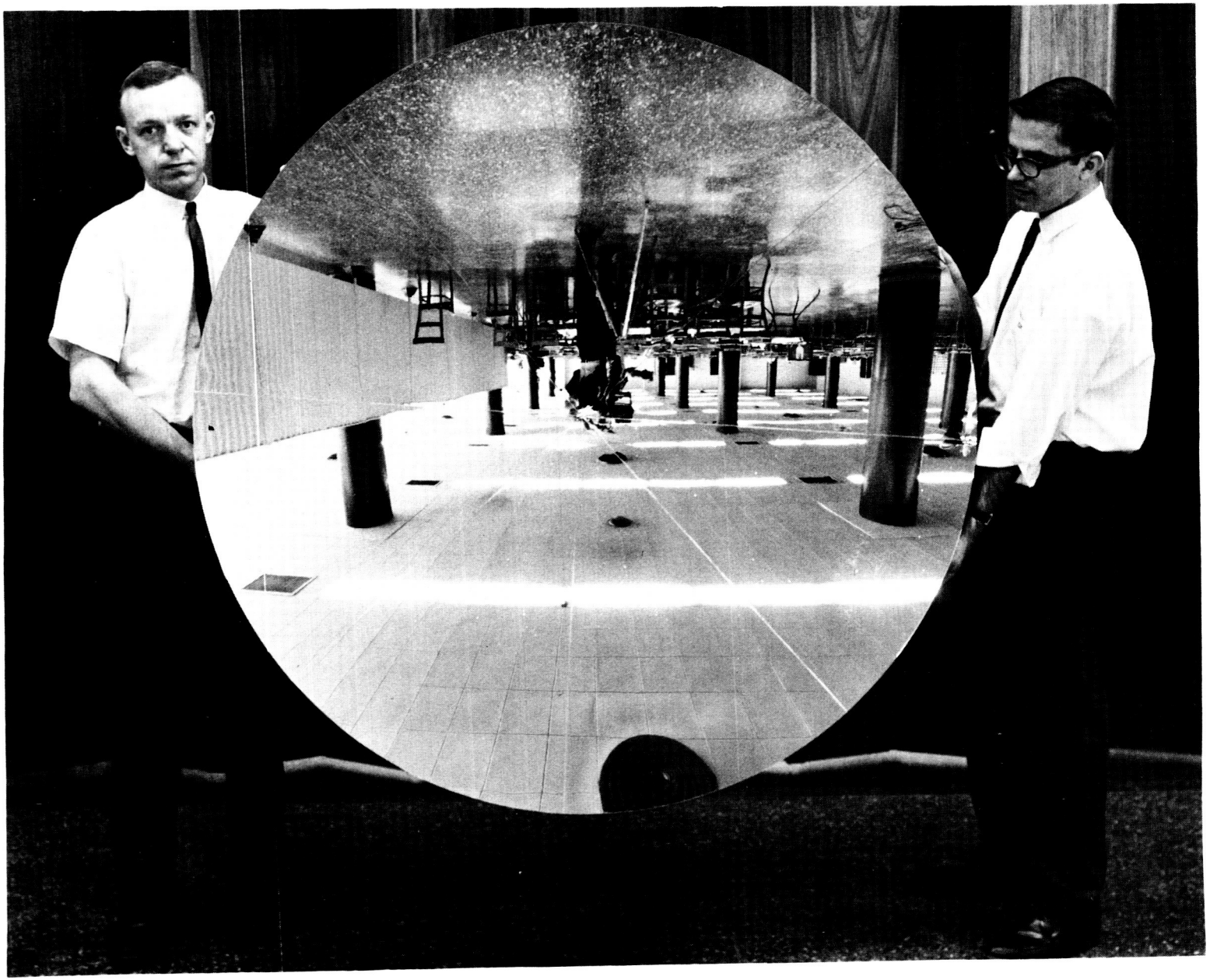

FIGURE 24
60 INCH DIAMETER SOLAR CONCENTRATOR

CONCENTRATOR OPTICAL QUALITY

The optical quality of a solar reflector can be represented by the geometric accuracy of the general surface with respect to a paraboloid and by the solar reflectivity. The 60-inch diameter solar concentrator which was fabricated under this contract is shown in figure 24, and the measured optical quality of this reflector will now be presented.

Geometric Quality

As discussed previously, the geometric quality of the reflector is obtained from the full size inspection photographs shown at reduced scale in figure 23. The mismatch of the grid patterns determines the surface error deviations while the completely white areas along the radial joints indicates surface area which may be optically lost - especially for high concentration ratio requirements. The majority of the white area at the outer diameter is due to the oversize photographic paper. The outer diameter edge distortion can be seen as the waviness around the exposure diameter.

Standard deviation of surface slope errors. -The mismatch data at discrete points on the inspection photographs were tabulated for the radial and circumferential errors. Although a cartesian grid is most apparent in figure 23, the fine radial reference lines were used to establish the center of the reflector, and the radial and circumferential components of error were read directly by pivoting a reference scale from this center.

Histograms for both directions are shown in figures 25 and 26, and as observed with previous solar concentrators, the normal distribution characteristic is apparent. The statistically determined mean values and standard deviations are tabulated below and compared with the values which were achieved on previously fabricated stretch-formed solar reflectors.

Concentrator	Radial		Circumferential		
Description	Mean	Std. Dev.	Mean	Std. Dev.	Reference
TRW S/N 2	3.7'	8.2'	-3.6'	11.0'	Ref. 6
TRW S/N 4	0.81'	2.86'	0.40'	3.77'	Ref. 7
Present	-0.45'	1.59'	0.50'	2.08'	Figure 23

The mean or average values may indicate that the reference system for measuring errors did not correspond to the best optical fit paraboloid. However, it is seen that these mean values are small and therefore they have a small effect upon the computed standard deviations.

Edge distortions. -The range of edge distortions in the free trimmed edges of the final hardware sectors was presented previously (figure 8). The degree to which this distortion was restrained by the radial splices can be seen in figure 23 by observing the white areas along the radial joints. From the full

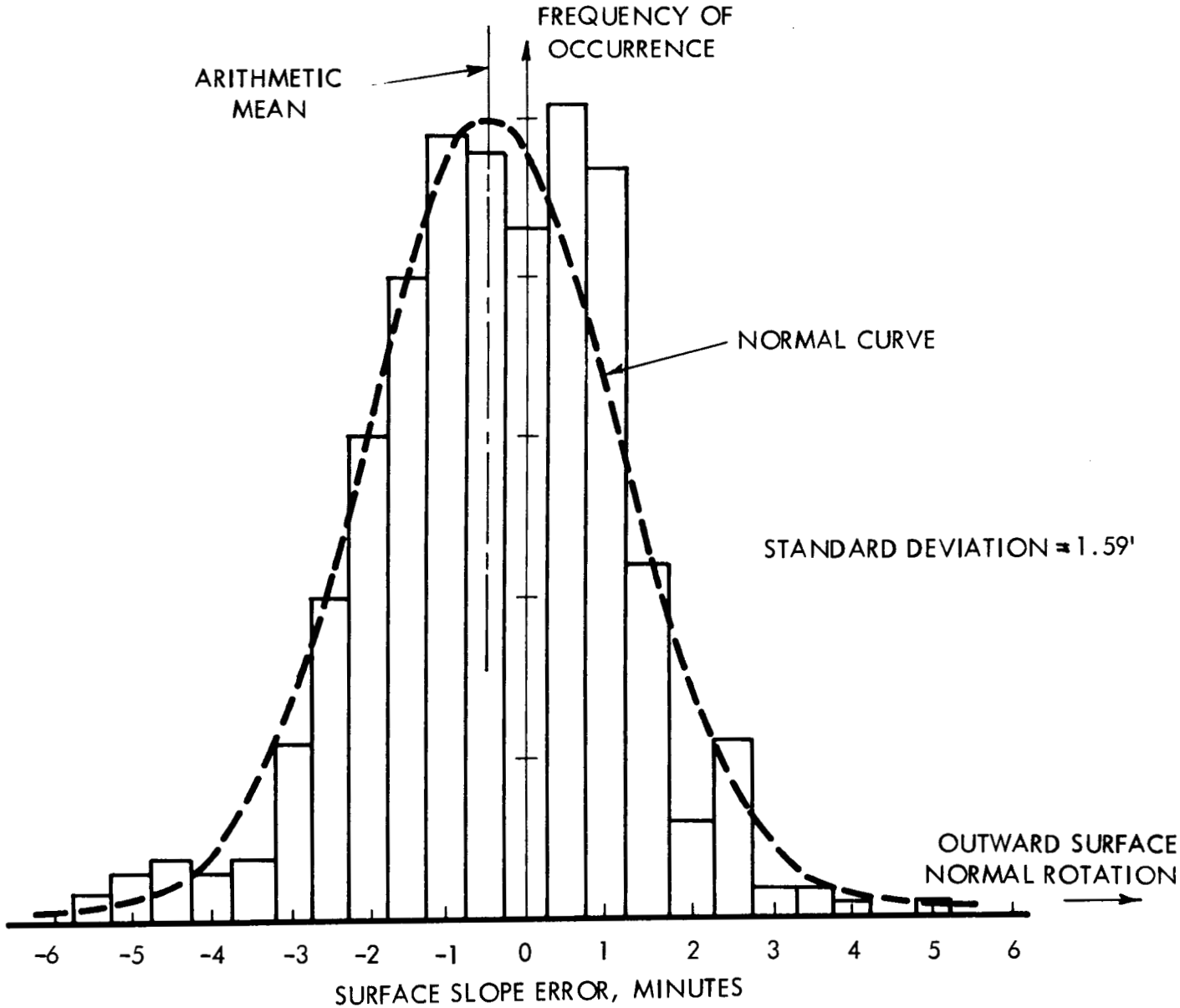

FIGURE 25
RADIAL ERROR FREQUENCY DISTRIBUTION

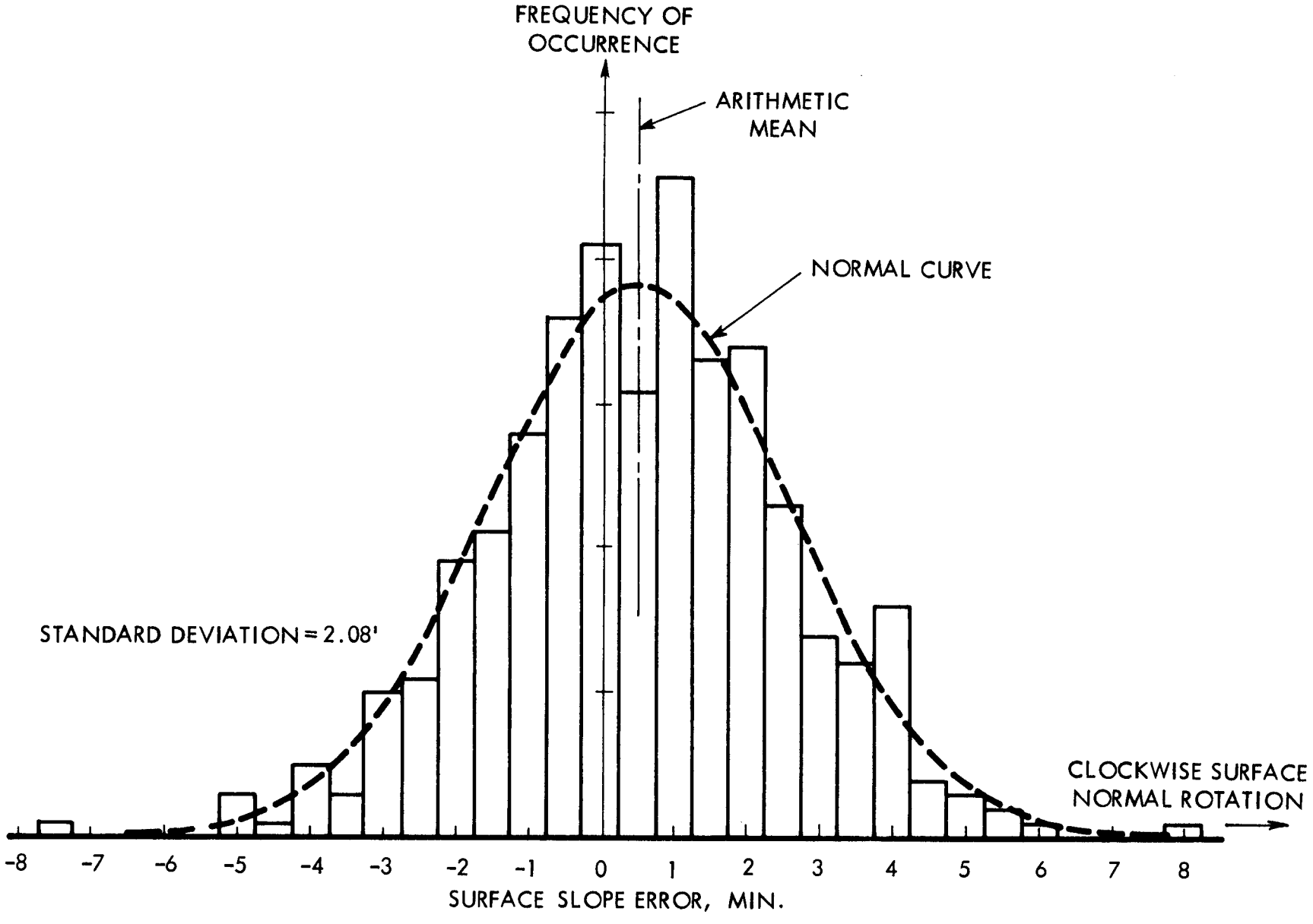

FIGURE 26
CIRCUMFERENTIAL ERROR FREQUENCY DISTRIBUTION

scale inspection photographs, this area was integrated and it composes 5% of the projected area of the 60 inch diameter reflector. Of the eight splice joints, the best joint condition contributed only 0.4% and the worst contributed approximately 1%.

The lost area at the outer diameter of the mirror was also integrated and composes approximtely 1.5% of the reflector area.

Thus, the combined area of the concentrator which is highly distorted is approximately 6.5%. A portion of this area can be interpreted to be represented by the tail of the normal distribution curves previously discussed; however, the majority of this area is probably lost with respect to solar concentration performance in the high concentration ratio region.

The highly distorted area represented by the 6.5% factor is approximately 1.3 sq. feet and this is estimated to be less than one-half the edge distortion previously observed on stretch-formed solar concentrators.

Reflectivity

Reflectivity specimens were cut from the trimmed portion of the final hardware panels. Three samples taken from the early, mid, and late portions of the vacuum aluminized period were measured for spectral directional reflectance and for the non-specular component of reflectivity at various wavelengths.

Since no silicon oxide top coating was used, the spectral directional reflectance characteristics of all specimens were almost identical. A typical spectral curve is shown in figure 27 in comparison to previously achieved results.

The integrated solar reflectivity, some typical total spectral reflectance values, and the non-specular components of reflectance for the three specimens which were measured during this contract are:

Sector Sample Number	Integrated Solar Reflectivity	Wavelength Microns	Total Spectral Reflectance	Non-Specular Component
3	89%	0.355	86.5%	0.2%
		.399	87.2	0.1
		.457	87.4	0.0
		.702	84.2	0.0
		1.002	92.0	0.0
		1.898	94.0	0.0
6	90%	0.355	87.2%	0.2%
		.399	89.0	0.1
		.457	88.8	0.0
		.702	84.0	0.0
		1.002	90.0	0.0
		1.898	95.0	0.0

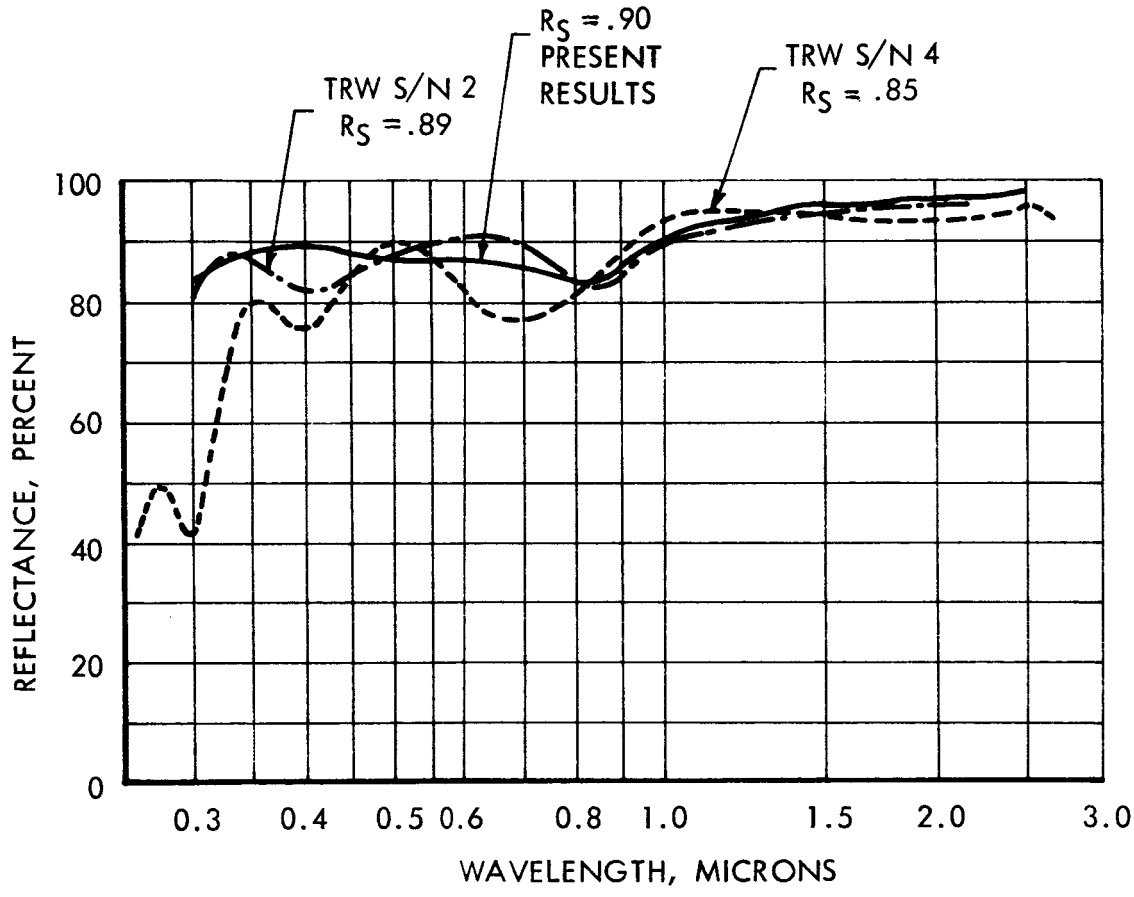

FIGURE 27
SPECTRAL REFLECTANCE

Sector Sample Number	Solar Reflectivity	Wavelength Microns	Total Spectral Reflectance	Non-Specular Component
7	89%	0.355	88.0%	0.9%
		.399	88.8	0.6
		.457	88.0	0.4
		.702	84.0	0.3
		1.002	92.0	0.2
		1.898	96.0	0.1

It is seen that the diffuse component is very low for all specimens, and would reduce the solar reflectivity by less than one-percent within the range of non-specular measurement capabilities of the reflectometer. An integrating sphere of the type described in reference 8 was used for all measurements.

CONCENTRATOR WEIGHT

In the application of one-piece solar concentrators to space solar power systems, weight is an important parameter which is often used to extrapolate and predict the comparable performance of these devices. Minimum weight, therefore, is one of the major objectives in the design and fabrication of space solar reflectors.

The achieved weight breakdown for the 60 inch concentrator shown in figure 24 is listed below.

Shell sectors	4.7 lbs	(calculated)
Radial joint strips	0.8	(calculated)
Tube torus	3.4	(measured)
Support inserts	0.1	(measured)
Skirt	0.9	(measured)
Adhesive and coatings	0.85	
Total measured weight	10.75 lbs.	(measured)

This weight results in a specific weight of 0.55 lb/sq. ft. of intercepted solar flux.

DISCUSSION, CONCLUSIONS AND RECOMMENDATIONS

A major portion of the contract effort was the improvement of the existing fabrication facilities and process. The resulting fabrication process, shown in Appendix A, outlines the important requirements for the fabrication of a light-weight, accurate solar concentrator using the stretch forming technique as the basic replication technique.

The 60 inch diameter solar concentrator which was fabricated by this process displays improvement over previous mirrors. The geometrical optical quality of 1.59 minutes and 2.08 minutes standard deviation of radial and circumferential surface errors demonstrates that the stretch forming technique

is an accurate method of replication.

The epoxy surface improvement spray coating has been improved. The present coating is more space compatible and more specular than others which have been investigated; however, this epoxy system displays a fine orange peel tendency and appears to be a poor "wetter". The random small crators in the coating due to this non-wetting are an undesirable surface blemish and further effort with other high temperature coating systems is recommended.

The new trimming support tool in conjunction with the existing high speed slitting saw method of cutting sectors was not successful in eliminating the edge distortion completely. However, with the aid of the joint reinforcing design, the 60 inch concentrator did display a reduced edge distortion characteristic. The estimated 6.5% distortion area is a major loss for high concentration ratio collectors and can be improved upon with the present design. For example, the best radial joint displayed only a 0.4% edge distortion and if obtained on all eight joints would reduce the total distorted area to 3.2% or less. Also, for larger diameter reflectors of the same proportions, the edge distortion increases linearly with the joint lengths while the percentage of edge distortion is inversely proportional to the intercepted area of the concentrator which increases as the square of the diameter. Thus for a 10 foot concentrator, the percent edge distortion would be one-half that of a 60 incher.

Edge distortion can be reduced by the obvious method of reducing the number of sectors in an assembly. Also, the cutting method and even the splicing operation can be further investigated to include development of EDM or abrasive cutting and ultrasonic or electron beam welding. Since these approaches will require large tooling expenditures, a preliminary study is recommended to investigate and compare the various new techniques.

The measured discontinuity stress level at the ring-shell junction is higher than anticipated. The value of 40 for the ratio of the measured discontinuity stress to the calculated membrane stress might be compared with those calculated by using various analytical approaches previously available in the literature for one-piece solar concentrators with ring stiffening. For example, reference 9 uses the analytical model of a built-in shell to calculate the discontinuity stresses and the resulting ratio of maximum meridional discontinuity stress to membrane stress is only 2. This indicates that the assumption of the support torus being rigid is not valid for light weight designs. The analysis of reference 10 uses the analytical model of a ring and shell where the ring is continuously supported but is allowed to increase in diameter and rotate. Compatibility equations are developed in terms of ring and shell influence coefficients from which the redundant forces and moments can be calculated. These redundant reactions on the shell result in discontinuity stresses with a ratio of approximately 15 for a typical light-weight ring design.

From these comparisons it is seen that an accurate analytical model of the shell-ring combination on three supports is not available. Such an analysis is recommended as the basis for ring and shell shape and weight optimization.

APPENDIX A

Fabrication Sequence For 60 Inch Stretched Formed Solar Concentrator

TOOLING SETUP

Align master stretching form to best geometric shape - use dial indicator arrangement.

Position clean air units and stock inspection table in front of stretching tool.

STRETCH FORMING

STOCK PREPARATION

Trim sheets to size with scissors.

Clean sheets - Use 2% Aerosol OT solution to wash thoroughly.

Rinse with tap water. Solvent wash by using generous amounts of Acetone. Solvent wipe with mixture of solvents.

Place cleaned sheets on handling tray with soft paper layer between. Never slide sheets, always pick up cleanly.

Move cleaned stock to stretch forming area.

STRETCHING

Clean glass master with solvents and inspect with light beam. Blow off any loose particle with air. Have laminar flow on continuously.

Using spray gun, spray fluorocarbon lube onto master. Allow to dry and remove any observed particles. Medium buff dry lubricant to uniform coating.

Place stock on table in front of clean bench. Inspect stock and tool for dust. Glove wipe.

Clamp sheet in jaws.

Inspect between stock and tool with bright light and blow off with air if necessary.

Clamp sheet in jaws.

Stretch at low rate - approximately 1 inch per minute.

Release pressure.

Using fixture, drill two holes at each end and scribe center.

Place contoured removal fixture on sheet and tape down.

Cut ends between apron and jaws and lift formed sheet from die.

Visually inspect part.

ETCHING BACK & CUTTING

Move sheet on removal fixture to trimming area, place on male tool and remove fixture.

Brush apply etching paste to back side of panel in radial splice areas and let dry.

Wash off with water and dry.

Brush coat with strippable coating to protect etched surface and let dry.

Place guide bar over sheet and cut in half with slitting saw.

Place each piece in carrying trays.

Remove burrs.

SURFACE IMPROVEMENT COATING

CLEANING

Wash panel with solvent mixture and dry.

Spray apply dilute etching paste to entire front surface of panel and let dry.

Wash off with water and watch for "water break". Surface should retain a continuous water film for a minimum of 30 seconds. Let dry. Move panel to spraying area.

SPRAYING

SPRAY EQUIPMENT PREPARATION

Dismantle spray guns and all fittings. Solvent clean and wipe dry and re-assemble.

Fit new fluid lines from reservoir to guns.

APPENDIX A

MIX EPOXY

100 PBW epoxy part A

60 PBW epoxy part B

47 PBW MIBK

47 PBW 2-butoxyethyl acetate

Mix thoroughly.

Filter mixture.

Place in spray reservoir.

SPRAY OPERATION

Check spray settings - air pressure - 75 psi
tank pressure - 10 psi
flow setting - 100
pattern setting - fan shape
gun travel - 50 fpm

Check spray pattern on fixture surface and adjust.

Wipe down spray fixture and booth with dust free cloth.

Mount part to be sprayed on rotating spray fixture.

Final wash part with solvent mixture (MIBK , 2-BUT).

Seal booth and dry part with lamps and filtered air blowers on. From this point, the spray booth remains sealed.

Recheck spray settings and automatically spray the part. Shut off system.

Rotate the part slowly (12 rpm) for 30 minutes to allow leveling.

Turn on heat lamps and allow this precure drying for approximately 12 hours.

Remove part from sealed spray booth and place in handling tray and cover with mylar for curing.

Cure part in oven - 150°F, 3 hours
300°F, 2 hours

Remove part from oven and transfer to aluminizing tank area.

APPENDIX A

VACUUM COATING

PREPARATION

Secure panel on metal tray and hang on dolly.

Blow off any loose particle or lint.

Load aluminum filaments with 4 to 5 clips.

Check and re-fill silicon oxide boats.

Close tank and pump down in 10^{-4} range.

GLOW DISCHARGE

Bleed in air to approximately 60 micron.

Glow discharge at 350 ma for 10 min.

Close bleeder valve.

SiO EVAPORATION

Pump down to 9×10^{-5} mm Hg

Open water valves for line cooling.

Close shutter.

Feed current at approximately 32 amps per active filament for 10 minute warm up period.

Open shutter and observe color change on control specimen till thickness is 1100Å. Deposition rate should be about 1-2 A°/sec.

Close shutter, shut off power.

ALUMINUM EVAPORATION

Pump down to 1×10^{-5} mm Hg

With shutter closed warm up filaments at approximately 40 amps per active filament until aluminum clips are melting.

Open shutter.

Increase power rapidly to 100 amps per active filament for not more than 10 sec.

Close shutter and cut power.

Open tank and visually inspect part.

Protective coat aluminized face with strippable coating.

TRIMMING

Place piece on clean trimming tool drop pins through holes into drill bushings in tool.

Pin side guide rail.

Use trimming saw and cut radial edge. Repeat on other side.

Tape down radial sides, pin center fixture, attach saw to arm and arm to center fixture.

Use trimming saw and cut outer diameter.

Place sector into tray and deburr.

Cover and move to assembly and inspection area.

SELECTIVE INSPECTION

Remove strippable coating.

Place sector on inspection rig and obtain grid photograph.

Compare all pictures and select the best 8 pieces for assembly.

Obtain total reflectance values for sectors to help in selecting the best pieces.

FINAL ASSEMBLY

RING & SKIRT SUBASSEMBLY

Etch and rinse previously formed ring and skirt elements.

Shim ring to proper location above master parabolic tool.

Final check fit of skirt to ring and skirt tabs to parabolic surface of tool.

Mix adhesive and paddle onto glass cloth tape.

Apply wet tape to skirt on ring tabs.

Fit skirt to ring and tape down.

Apply elastic cord to skirt outer circumference to hold in place for curing.

Room cure for 24 hours.

Remove ring-skirt subassembly from tool.

SHELL SUBASSEMBLY

Position 8 trimmed sectors on master tool in optical inspection rig.

Remove strippable coating from back at splice joint location.

Tape seal radial seam with 1/8 wide tape and final wipe joint area.

Mix adhesive and paddle into glass cloth tape.

Apply wet tape to previously cut splice lap strips.

Apply strips to radial joints.

Bag over entire shell with polyethylene. Seal at OD of tool.

Pull vacuum under bag and room cure for 24 hours.

Remove vacuum bagging.

FINAL ASSEMBLY

Seal the shell at its OD and pull vacuum between shell and glass master.

Remove strippable coating from shell OD and final wipe.

Mix adhesive and paddle into glass cloth tape.

Apply wet tape to skirt tabs.

Fit ring and skirt subassembly to shell and tape down.

Dead weight ring lightly and room cure for 24 hours.

Remove weights and sealing material when cured.

FINAL INSPECTION

Attach mounting fixtures to ring supports.

Remove master glass tool which was used for assembly.

Realign optical inspection setup.

Obtain grid inspection photographs.

APPENDIX B

Spray Coating Optimization Results

Epoxy: Solvent Ratio	Solvent System	Leveling Speed RPM	Precure Time Hrs.	Cure Temp °F	Cure Time Hrs.	Results & Comments
2:1	25% MEK 25% TOL 25% MIBK 25% 2-BUT	24	1.5	175 300	3 4	Sharp orange peel
1:33:1	25% MEK 25% TOL 25% MIBK 25% 2-BUT	24	1.5	175 300	3 4	Med. orange peel
2.5:1	33% MEK 33% TOL 33% MIBK	24	1.3	200 300	3 3	Gross orange peel
2:1	33% MEK 33% TOL 33% MIBK	24	1.3	200 300	3	Gross orange peel
2.5:1	33% TOL 33% MIBK 33% 2-BUT	24	3.6	200 300	2.5 2	Sharp orange peel
2:1	33% TOL 33% MIBK 33% 2-BUT	24	3.3	200 300	2.5 2	Med. orange peel, streaks
3:1	33% MIBK 33% 2-BUT 33% MEK	24	2.0	200 300	2 2	Sharp orange peel
2.5:1	33% MIBK 33% 2-BUT 33% MEK	24	2.0	200 300	2 2	Med. orange peel, streaks
4:1	33% 2-BUT 33% MEK 33% TOL	24	2.8	200 300	3 5.5	Sharp orange peel, small bubbles
3:1	33% 2-BUT 33% MEK 33% TOL	24	2.8	200 300	3 5.5	Med. orange peel, thermal tested
5:1	50% MEK 50% 2-BUT	24	3.0	200 300	2 5.5	Sharp orange peel

APPENDIX B

Epoxy: Solvent Ratio	Solvent System	Leveling Speed RPM	Precure Time Hrs.	Cure Temp °F	Cure Time Hrs.	Results & Comments
3.5:1	50% MEK 50% 2-BUT	24	2.5	200 300	2 5.5	Med. fine o.p. Thermal tested
4:1	50% TOL 50% 2-BUT	24	1.5	200 300	2 5.5	Gross orange peel, streaks
3:1	50% TOL 50% 2-BUT	24	1.3	200 300	2 5.5	Gross orange peel, fine bubbles
4:1	50% MIBK 50% 2-BUT	24	4.0	200 300	1.5 2	Sharp orange peel
3:1	50% MIBK 50% 2-BUT	24	4.0	200 300	1.5 2	Med. orange peel
2:1	25% MEK 25% TOL 25% MIBK 25% 2-BUT	10	1.3	200 300	1.5 4	Sharp orange peel Runs
2:1	33% MEK 33% TOL 33% MIBK	10	3.0	200 300	3 2	Did not cover
3.5:1	50% MEK 50% 2-BUT	10	2.5	200 300	3 2	Did not cover
2.5:1	33% MEK 33% 2-BUT 33% MIBK	10	1.0	200 300	5 2	Sharp orange peel
3:1	50% TOL 50% 2-BUT	10	1.5	200 300	3 2	Did not cover
2:1	33% TOL 33% 2-BUT 33% MIBK	10	1.0	200 300	3 2	Med. orange peel Runs
3:1	33% 2-BUT 33% MEK 33% TOL	10	2.0	200 300	3 2	Sharp orange peel
3:1	50% MIBK 50% 2-BUT	10	2.0	200 300	3 2	Fine orange peel. Thermal tested-cracked

APPENDIX B

Epoxy: Solvent Ratio	Solvent System	Leveling Speed RPM	Precure Time Hrs.	Cure Temp °F	Cure Time Hrs.	Results & Comments
2:1	2-BUT	24	0.5	200 300	2 2	Coating cracked at edge, sharp o. p.
1.33:1	25% MEK 25% TOL 25% MIBK 25% 2-BUT	44	4.0	200 300	3 2	Fine orange peel
2:1	33% MEK 33% TOL 33% MIBK	44	3.5	200 300	3 2	Gross orange peel, Runs
3:1	50% MEK 50% 2-BUT	44	3.0	200 300	3 2	Med. orange peel, Thermal tested
2.5:1	33% MEK 33% 2-BUT 33% MIBK	44	2.5	200 300	3 2	Med. orange peel
3.5:1	50% BUT 50% 2-BUT	44	2.3	200 300	3 2	Med. orange peel Streaks
3:1	50% TOL 50% 2-BUT	44	2.0	200 300	2 2	Elongated o. p.
2:1	33% TOL 33% 2-BUT 33% MIBK	44	1.5	200 300	2 2	Elongated o. p.
3:1	33% 2-BUT 33% MEK 33% TOL	44	1.5	200 300	2 2	Sharp orange peel, Streaks
3:1	50% MIBK 50% 2-BUT	44	1.0	200 300	2 2	Med. orange peel
2.5:1	Butanol	0	0	150 300	12 2	Deep orange peel
1.5:1	20% 2-BUT 80% BUT	0	0	72	24	Surface crazed completely

APPENDIX B

Epoxy: Solvent Ratio	Solvent System	Leveling Speed RPM	Precure Time Hrs.	Cure Temp °F	Cure Time Hrs.	Results & Comments
1.5:1	10% MEK 10% MIBK 10% TOL 20% 2-BUT 50% BUT	0	3.0	150 300	12 2	Med. orange peel Too thin
3:1	50% MIBK 50% 2-BUT	12	1.5	150 300	20 2	Fine orange peel
2.5:1	50% MIBK 50% 2-BUT	0	12	150 300	6 2	Fine orange peel Runs
2:1	50% MIBK 50% 2-BUT	12	2.5	150 300	64 2.5	Fine orange peel, Thermal tested
2.4:1	50% MEK 50% 2-BUT	12	2.0	150 300	64 2.5	Fine orange peel
2.4:1	40% MEK 40% 2-BUT 20% Resin	0	0	150 300	48 2.5	Fine orange peel Runs
2.4:1	40% MEK 40% 2-BUT 20% Resin	12	24	150 300	2 2.5	Fine orange peel, Thermal tested
2:1	48% MIBK 48% 2-BUT 4% Resin	12	24	150 300	2 2.5	Fine orange peel
2:1	50% MIBK 50% 2-BUT	12	2	150 300	3 2.5	Fine orange peel, Thermal tested
2.3:1	25% MIBK 75% 2-BUT	12	0	150 300	3 2.5	Med. orange peel, Thermal tested
2.3:1	2-BUT	12	3	150 300	3 3	Fine orange peel, Thermal tested

APPENDIX B

Epoxy: Solvent Ratio	Solvent System	Leveling Speed RPM	Precure Time Hrs.	Cure Temp °F	Cure Time Hrs.	Results & Comments
1.7:1	17% TOL 33% XYL 33% BUT 14% 2-BUT 3% MIBK	12	1.0	150 300	2 3	Too thin Thermal tested
1.8:1	2-BUT	12	12	150 300	2 3	Med. orange peel
1.7:1	50% MIBK 50% 2-BUT	12	12	150 300	2 2	Fine orange peel, Thermal tested

REFERENCES

1. 60 Inch Stretch-Formed Aluminum Solar Concentrator. NASA CR-47, June 1964.

2. Timoshenko, S.; and Woinowsky-Krieger, S.: Theory of Plates and Shells. Second ed., McGraw-Hill Book Co., Inc., 1959.

3. Pfluger, Alf.: Elementary Statics of Shells. Second ed., McGraw-Hill Book Co., Inc., 1954.

4. Roark, Raymond J.: Formulas for Stress and Strain. Third ed., McGraw-Hill Book Co., Inc., 1954.

5. Sunflower Solar Collector Topical Report. NASA CR-46, May 1964.

6. Analysis of Solar Reflectors Mathematical Theory and Methodology for Error Model Synthesis from Experimental Ray Trace Data. Allison Division, GMC, EDR 3958, September 1964.

7. Schrenk, G. L.; and Lowi, A.: Mathematical Simulation of Solar Thermionic Energy Conversion Systems. Proceedings of the International Conference on Thermionic Electrical Power Generation, IEE Meeting, London, September 20-24, 1965.

8. Edwards, D. K.; Gier, J. T.; Nelson, K. E.; and Roddick, R. D.: Integrating Sphere for Imperfectly Diffuse Samples. J. O. S. A., Volume 51, Number 11, 1279-1288, November 1961.

9. Schmidt, Ferenc J.; and Hess, Irving J.: Electroforming Aluminum for Solar Energy Concentrators. NASA CR-197, April 1965.

10. Brayton Cycle Solar Collector Design Study. NASA CR-54118, March 1964.